

## **Greenhouse heating by energy transfer between greenhouses: System design and implementation**

Weituo Sun <sup>a,b</sup>, Xiaoming Wei <sup>a</sup>, Baochang Zhou <sup>a,c</sup>, Chungui Lu <sup>b,\*</sup>, Wenzhong Guo <sup>a,\*</sup>

<sup>a</sup> Intelligent Equipment Research Center, Beijing Academy of Agriculture and Forestry Sciences, Beijing 100097, China

<sup>b</sup> School of Animal, Rural and Environmental Sciences, Nottingham Trent University, Nottinghamshire NG25 0QF, UK

<sup>c</sup> College of Horticulture, China Agricultural University, Beijing 100094, China

\* Corresponding authors.

E-mail address: guowz@nercita.org.cn (Wenzhong Guo); chungui.lu@ntu.ac.uk (Chungui Lu)

Nomenclature			
		$\alpha_{ts}$	binary switch function (-)
Latin symbols		$\beta_{hp}$	extra coefficient for heat pump selection (-)
$A$	area (m <sup>2</sup> )	$\beta_{sac}$	correction coefficient for surface air cooler selection (-)
$CDH$	conductive heat flux (W m <sup>-2</sup> )	$\delta$	thickness (m)
$COP$	coefficient of performance of heat pump (-)	$\Delta$	Difference; low deviation for setpoints
$c_p$	specific heat at constant pressure (J kg <sup>-1</sup> °C <sup>-1</sup> )	$\varepsilon$	long-wave radiation emissivity of surfaces (-)
$CTH$	one-through or combined heat flux (W m <sup>-2</sup> )	$\zeta$	total transmittance of south roof to solar radiation (-)
$CVH$	convective heat flux (W m <sup>-2</sup> )	$\theta$	angle (°)
$E$	input electric power of heat pump (W)	$\theta_{crl}$	angle between $L_{crl}$ and north wall (°)
$F$	view factor (-)	$\lambda$	thermal conductivity (W m <sup>-1</sup> °C <sup>-1</sup> )
$g_{v,leak}$	specific ventilation rate due to infiltration (m s <sup>-1</sup> )	$\rho$	density (kg m <sup>-3</sup> )
$g_{v,roof}$	specific ventilation rate due to roof ventilation (m s <sup>-1</sup> )	$\sigma$	Stefan-Boltzmann constant (W m <sup>-2</sup> K <sup>-4</sup> )
$h$	convective heat transfer coefficient (W m <sup>-2</sup> °C <sup>-1</sup> )	$\tau$	transmittance to long-wave radiation (-)
$H$	average height of multi-span greenhouse (m)	$\phi$	fan output frequency (Hz)
$H_C$	average height of CSG (m)		
$H_g$	height of greenhouse sidewall excluding foundation wall (m)	Subscripts	
$HP$	heating capacity (heat output) of heat pump (W)	a	ambient (outdoor) air
$H_{rid}$	CSG ridge height (m)	air	air
$I$	solar radiation received by surfaces (W m <sup>-2</sup> )	c	greenhouse cover (envelope)
$I_{com}$	compressor running current (A)	c11	connecting line between roof ridge and bottom angle of north wall
$k$	comprehensive heat transfer coefficient from internal surface of envelop to outdoor air (W m <sup>-2</sup> °C <sup>-1</sup> )	c12	connecting line between bottom angle of south roof and apex of north wall
$L$	greenhouse length; characteristic length (m)	com	compressor
$L_v$	open width of CSG roof vents	cs	soil of constant temperature
$N$	infiltration rate of multi-span greenhouse (h <sup>-1</sup> )	d	dual source
$N_C$	infiltration rate of CSG (h <sup>-1</sup> )	f	greenhouse floor
$pe$	greenhouse perimeter (m)	f,out	Outdoor ground
$p_{ts}$	energy-saving fraction of indoor thermal screen (-)	fC	CSG floor
$Q_h$	multi-span greenhouse heating load (W m <sup>-2</sup> )	g	greenhouse air; indoor radiating body
$Q_{nw}, Q_{nr}, Q_{sr}, Q_{jC}$	convections of internal surfaces of north wall, north roof, south roof, and indoor floor (W m <sup>-2</sup> )	gC	CSG air
$Q_s$	CSG surplus air heat (W m <sup>-2</sup> )	i	each layer
$Q_{tr}$	combined heat transfer through envelope (W m <sup>-2</sup> )	in	internal surface
$Q_v$	air infiltration heat loss (W m <sup>-2</sup> )	inl	inlet water of heat pump condenser (°C)
$Q_{vC}$	Heat transfer by CSG air exchange (W m <sup>-2</sup> )	ins	installed capacity
$r^*$	apparent radiation heat transfer coefficient (W m <sup>-2</sup> °C <sup>-1</sup> )	low	lower limit
$RSH$	radiative heat flux between surfaces (W m <sup>-2</sup> )	nr	north roof of CSG
$RTH$	radiative heat flux between surface and sky (W m <sup>-2</sup> )	nw	north wall of CSG
$SAC$	rated heat dissipating capacity of surface air cooler (W)	out	external surface
$t$	temperature (°C)	outl	outlet water of heat pump condenser (°C)
$t_{a,1}, t_{a,2}, t_{a,3}$	hierarchical design temperatures of outdoor air (°C)	rc	rated condition
$TD_g$	time duration for heating multi-span greenhouse (h)	sky	sky
$TD_{gC}$	time duration for collecting CSG surplus air heat (h)	soil	soil
$t_{g,1}, t_{g,2}, t_{g,3}$	hierarchical design temperatures of indoor air (°C)	sr	south roof of CSG
$U$	overall heat transfer coefficient (W m <sup>-2</sup> °C <sup>-1</sup> )	sun	solar altitude
$U_{com}$	compressor operating voltage (V)	t	pass through cover
$v$	outdoor wind speed (m s <sup>-1</sup> )	ta	at the outdoor air temperature of $t_a$
$V$	effective volume (m <sup>3</sup> )	tank	heat storage tank
$v_{gC}$	wind speed inside CSG (m s <sup>-1</sup> )	up	upper limit
$v_{hp}$	flow rate of circulating water passing through heat pump (m <sup>3</sup> h <sup>-1</sup> )	w	water
$W$	greenhouse width (m)		
		special characters	
Greek symbols		,	further limitations for the content before it
$\cos\phi$	power factor of compressor (-)	_	heat flux from the former to the latter
$\alpha$	absorption ratio to solar radiation (-)		

## Abstract

Multi-span greenhouses consume enormous amounts of energy for heating in northern China, resulting in poor profitability and unsustainability. A greenhouse heating system, utilizing energy transfer between greenhouses based on a dual source heat pump, was designed to remedy this issue. The system collects surplus air heat inside Chinese solar greenhouses (CSGs) for heating multi-span greenhouses. Through enabling a greenhouse energy transfer in time and space, improved utilization efficiency of surplus air heat in CSGs is achievable, resulting in an overall reduction of heating costs. This study defines the heating approach and describes the overall system design. The dual source heat pump acts as the core component, with two separate evaporators placed in the CSG and ambient air. Calculations for system sizing are then presented, including a heating load model of multi-span greenhouses, a surplus air heat model of CSGs, the selection of required equipment (dual source heat pump, heat storage tank, and surface air cooler of the combined air conditioning unit), and the area matching. Finally, a case study illustrates the implementation processes of the heating system. The available CSG surplus air heat ranged 100.8-112.6 W m<sup>-2</sup> for system sizing, and the minimum area of CSGs was suggested to be twice the multi-span greenhouse area. The pilot test showed that the running status and heating effect of the system was stable. The coefficient of performance (COP) of the heat pump reached 4.3-4.8 when using CSG surplus air heat as the heat source, performing 23-26% higher than when using ambient air over the same periods. Throughout the entire course of heat collection, dual source heat pumps, switching sources based on their setting, achieved a total COP of 3.4-4.2, increased by 6-11% compared with air source heat pumps. This study provides a novel heating approach and an energy-saving system for multi-span greenhouses.

**Key words:** Greenhouse heating, Chinese solar greenhouse, heat pump, energy transfer, surplus heat, heating load

## **1. Introduction**

### **1.1. General background and motivation**

Across China, the greenhouse horticulture industry has recognized the expansion of large-scale greenhouses as a strategy for market development. One such representative is the multi-span greenhouse, which demonstrates high efficiency of land use, strong ability of climate control, and a high level of mechanized operation. Such features enable multi-span greenhouses to be suitable for scaled and commercial production. However, multi-span greenhouses consume enormous amounts of energy for heating, especially during the cold seasons in northern China. The requirement for these high energy inputs is inefficient, resulting in poor profitability and unsustainability. The energy required for heating a greenhouse accounts for 30-70% of total greenhouse production costs, depending on different latitudes [1]. According to our investigations and greenhouse management practices, the annual heating cost of a multi-span greenhouse in Beijing is 6.3-12.5 US\$ m<sup>-2</sup>, accounting for more than 40% of the total operation cost. Across milder climates where multi-span greenhouses are well-developed, e.g. the Netherlands, greenhouse heating is also a significant energy consumer. The annual consumption of natural gas, which is the primary heat source for greenhouse heating, ranges from 25 to 40 m<sup>3</sup> m<sup>-2</sup>, with an average cost of 7.8 US\$ m<sup>-2</sup> [2, 3].

An overview of different energy-saving techniques for reducing greenhouse heating costs is provided by Ahamed et al. [4]. These measures that reduce either the heating demand or direct energy input mainly include design optimization of the greenhouse and its structural components [5, 6], improving greenhouse climate management [7-10], and utilizing renewable energy or energy-efficient technologies to decrease the consumption of fossil fuel or heating power [11]. At the beginning developing stage of the multi-span greenhouse industry in China, one of the most potent remedies for the greenhouse heating issue is to create an energy-saving, cost-effective, and stable heating approach and develop the required supporting equipment.

### **1.2. Research background and problem definition**

Heat pump technology, which features high energy conversion efficiency, low operating cost, and is considered environment-friendly, has been successfully used in greenhouse heating [12-19]. Moreover, it will play an increasingly important role as we follow stricter requirements for decreasing CO<sub>2</sub> emissions [2]. For example, the heating cost of a heat pump with a COP of 3.5 is slightly higher than a coal-fired

boiler, however still far below the natural gas boiler and electrical heating [20]. Meanwhile, the heat pump has the lowest primary energy consumption and CO<sub>2</sub> emissions [20]. In addition, compared with solar thermal systems [21, 22], the heat pumps have more stable heating performances, which is very important for crop safety production. In recent years, air source heat pumps, as the most widely used heat pump types [23], have been chosen for heating more and more multi-span greenhouses in China, since they are relatively inexpensive and stable, and easy to install and maintain. Nevertheless, the decreased heating capacity and low COP in cold weather [24] remain challenges for the efficient use of air source heat pumps. As the heat source quality largely determines the COPs [13, 24, 25], the energy-saving greenhouse heating by air source heat pumps puts forward a solid requirement to make full use of the higher-grade sources in cold regions that can hardly be scaled up in practical terms.

Alongside growing crops, greenhouses also harvest energy. For instance, the annual cumulative surplus energy inside an ideal closed greenhouse reaches 164 kW h m<sup>-2</sup> [26]. Recovering excess heat energy from a greenhouse in the daytime and supplying it for heating the greenhouse itself at night has been proved as a solution to improve the nighttime thermal environment [27], increase crop yield [28], and save energy [29]. However, during the coldest months in cold regions or high latitudes, the excess daytime heat inside commercial greenhouses (below 0.5 MJ m<sup>-2</sup> d<sup>-1</sup> on most days) contributes very little to the greenhouse heating requirement [29], while the energy excess mainly exists at the supplemental lighting phase or in warm seasons [30]. Such excess heat produced by artificial lights is unsustainable and can be cut down by a transition from high-pressure sodium (HPS) to light emitting diode (LED) lighting [31]. In addition, seasonal thermal energy storage is not a preferable choice due to its high investment cost [32]. In principle, it is inadvisable to extract excess energy from multi-span greenhouses for heating in cold areas, especially within a daily heat storage-release pattern.

Energy-saving and low-cost, the Chinese solar greenhouse (CSG) is the primary choice of greenhouse for overwintering cultivation in northern China. The total area of CSGs exceeded 570,000 hm<sup>2</sup> by the end of 2018, accounting for approximately 30.5% of the total greenhouse area in China [33]. Because of the unique north wall, the CSG has good thermal insulation and solar radiation interception performance. Consequently, the indoor air temperature can easily reach and exceed 35 °C around noon, even in winter months, creating an abundant surplus of air heat. In practice, roof ventilation cools the CSG and prevents crops from high-temperature stress. However, at the same time, excess energy is wasted in the process. Researchers have developed many active and passive heating systems to utilize surplus air heat energy or both excess solar radiation and air heat inside CSGs. The active solar heat storage-release systems are the most studied, which transfer and store energy through water circulation [34-38]. They focused on

improving the heat collection efficiency of indoor collectors while considering the heat release capacity. Other common practices utilizing CSG excess energy include the ventilated walls [39, 40], water-flowing roof skeleton network [41], and walls with phase change material (PCM) [42, 43] and heat conduction components [44]. Although these systems are low-cost, energy-saving, and benefit greenhouse climate and crop growth, they have a common technical issue, the effective heat collection time and total heating capacity are restricted by the temperature increase of the heat transfer and storage medium to varying degrees. The reason is that their heat capture depends on or is affected by the convection processes with indoor air. This issue results in low use efficiency of CSG excess energy.

Compared with the ambient air source, surplus air heat inside the CSG is higher-grade heat energy and particularly valuable during cold winters. This surplus energy can be harvested and considered the low-temperature heat source of a heat pump to improve COPs. Also, owing to forced extraction by the heat pump, a positive temperature difference will be efficiently formed between the heat storage medium and indoor air. In order to solve the limitations of the above CSG energy utilization systems in terms of heating capacity and energy use efficiency, different from the complex heat pump systems that extract greenhouse energy indirectly [29, 45], Sun et al. [46] developed a heat pump system with a single source of surplus air heat for CSG heating. The developed system enabled the heat pump to increase heating performance, with the overall COP of the heating system reaching 2.7. The results indicate that collecting the CSG surplus air heat directly by the heat pump during the daytime to heat the CSG itself at night is effective for greenhouse production.

However, to improve the utilization efficiency of the excess energy inside CSGs, previous studies focused on how to absorb more heat from the energy source under predefined constraints, and took into account the heat release performance of the heating system itself, but never considered the arrangement of energy sinks that could efficiently digest the obtained heat. Imbalances between the heat supply and demand can occur due to the thermal energy storage of CSG structures and that within the soil, especially in well-insulated CSGs. On sunny days where a vast amount of excess heat energy exists, the CSG heating requirement for night supplementation is reduced or not even required. In this case, the stored energy cannot be sufficiently consumed that night [37], adversely affecting heat collection during the day. The low heat requirement of CSGs can also be verified by the fact that the CSG can produce vegetables and fruits in Northern China (32-43° N) mostly without additional heating [47]. As a result, based on the existing systems, the heating approach that captures excess indoor energy during the daytime and releases that heat at night for heating the CSG itself has low efficiency on energy use, in view of the energy supply chain. Compared to CSGs, multi-span greenhouses have a higher heating load [48]; the daily heating cost

per unit area of the multi-span greenhouse was tested to be roughly 3.6 times that of the CSG during the entire heating period [17]. Moreover, their heating needs are nearly not affected by outdoor weather once entering the heating season. Therefore, collecting CSG surplus heat on sunny days to provide heating for multi-span greenhouses could improve overall CSG energy use efficiency and reduce heating costs of multi-span greenhouses by using alternative energy sources. Thus, in this study, we put forward a novel heating approach that utilizes energy transfer between greenhouses. However, no supporting system is available to implement this heating approach.

### **1.3. Objective and contributions**

In order to address the issues and take the opportunities, the project aims to develop a greenhouse heating system, utilizing energy transfer between greenhouses based on a dual source heat pump (ETGHP). The system collects surplus air heat inside CSGs for heating multi-span greenhouses. It is expected to enable greenhouse energy transfer in time and space by efficient use of the air source heat pump, and improve the utilization and efficiency of the CSG surplus air heat. Achieving this would then reduce the energy consumption for heating multi-span greenhouses, and promote the sustainable development of large-scale greenhouses represented by the multi-span greenhouse.

The development of greenhouse energy utilization systems, in previous studies, put more effort into the overall system description and performance evaluation, and few involved the detailed design of key equipment, system sizing, and implementation. At the same time, design calculations for the heat pump systems mainly focus on the internal configuration [49, 50]. A reliable heating load model applying to select air source heat pumps for greenhouse cultivation is unavailable. So first, a research gap exists in the framework that the design of the heating approach utilizing energy transfer between greenhouses, especially that practiced by the ETGHP system, can follow. Second, the dual source heat pump, the core component of the system, differs from the most commonly used solar/air [51, 52] and ground/air [53, 54] techniques. It needs a custom design for stable and energy-efficient heating purposes. Third, studying system implementation benefits engineering application and knowledge discovery of the heating approach. Therefore, this paper focuses on the design and implementation of the ETGHP system. The main contributions and innovations are as follows:

- (1) Proposing a heating approach that utilizes energy transfer between greenhouses and developing the ETGHP system to practice this approach.
- (2) Designing a dual source heat pump, which has two separate evaporators respectively placed in

the CSG and ambient air and performs three operating conditions, ensuring energy-saving and stable heating.

- (3) Establishing a systematic sizing method orienting to the engineering design of the ETGHP system, which contains a heating load model of multi-span greenhouses, a surplus air heat model of CSGs, and equipment selection, improved in the theoretical aspect.
- (4) Studying implementation processes and performing a pilot test of the system, from which we answer the following research questions:
  - How much is surplus air heat available in CSGs?
  - How large can the area of heat source CSGs match the multi-span greenhouse to be heated?
  - To what degree the heat pump COPs can be improved by using the CSG air source?

The rest of this paper is as follows: in section 2, the heating approach is defined, followed by the overall system design. Section 3 presents calculations for the heating load model, a surplus air heat model, and equipment selection. In section 4, we illustrate the system implementation process by case study. In addition, a pilot test was conducted to analyze the system's running status and heating effect, as well as the performance of heat pumps. Discussions run through this section, ending with a description of perspective and further study. Conclusions are made in section 5. This paper could provide theoretical support and be used as a case reference for the design and application of the ETGHP system.

## **2. System description**

### **2.1. Approach proposition**

The heating approach, utilizing energy transfer between greenhouses, is defined as collecting surplus heat energy inside one or more greenhouses to heat the other, one or more, greenhouses. There are several purposes for the proposition of this heating approach; a greenhouse energy transfer in time and space can be enabled, improving the energy use efficiency of surplus greenhouse heat energy, and reducing overall energy consumption for heating. The two types of greenhouses involved can be different greenhouse types, such as CSGs coupled with multi-span greenhouses. They can also be the same greenhouse types cultivating various crops, such as lettuce and tomato greenhouses. Heat collection methods mainly include extracting indoor air heat and intercepting incident radiation directly. Specifically, they can be forced extraction by a heat pump, forced convection by a heat exchanger, and solar energy collection. This study designs an ETGHP system to practice this greenhouse heating approach by extracting surplus air heat in CSGs and using it for multi-span greenhouse heating.

## 2.2. Overall design of the ETGHP system

As shown in Fig. 1, the ETGHP system consists of the dual source heat pump unit, a heat storage tank, heat release equipment (fan and surface air cooler, etc.), the ventilating duct, water pump, circulating water pipe, and the control system.

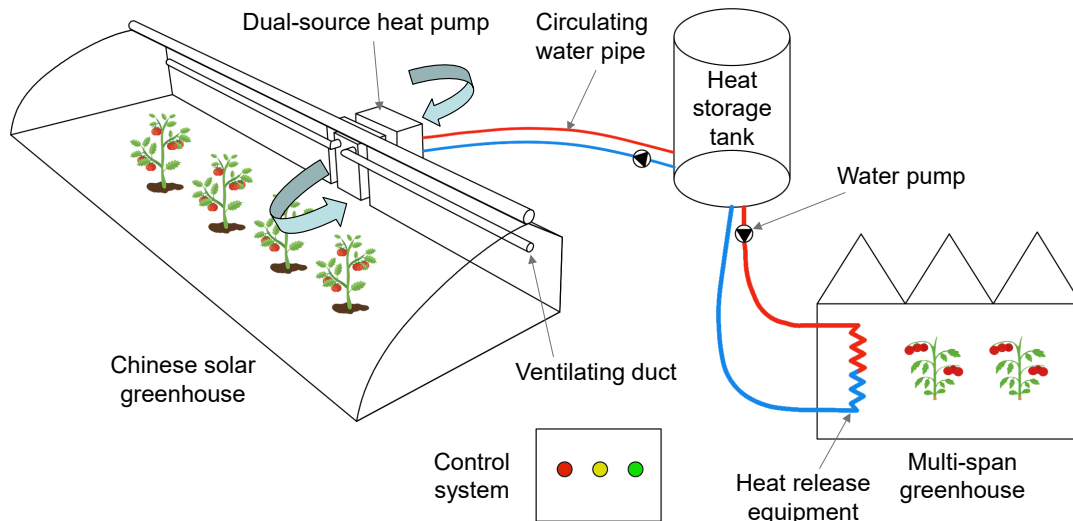


Fig. 1 Schematic diagram of the greenhouse heating system utilizing energy transfer between greenhouses based on a dual source heat pump

The dual source heat pump (Fig. 2) is the core component of the system. It has two sets of evaporators, each individually placed in the CSG and ambient air, respectively. This configuration enables the heat pump to have double heat sources, CSG air and ambient air. The two sources are switched by manipulating two expansion valves. During the building process, indoor evaporators and fans of the heat pump are embedded in the north wall of the CSG. Using a high-power compressor is preferred to modularize the heat pump. The dual source heat pump has the following three running conditions:

1. CSG air source heating condition: Solenoid valves 1 and 2 are closed, electronic expansion valve 2 is electrified, and electronic expansion valves 1 and 3 are not electrified. Loop of the heat pump working fluid is compressor → four-way reversing valve → shell and tube heat exchanger → check valve 5 → liquid reservoir → dry filter → plate heat exchanger → electronic expansion valve 2 → indoor finned tube heat exchanger → check valve 4 → four-way reversing valve → gas-liquid separator → compressor.

2. Outdoor air source heating condition: Solenoid valves 1 and 2 are closed, electronic expansion valve 1 is electrified, and electronic expansion valves 2 and 3 are not electrified. Loop of heat pump working fluid is compressor → four-way reversing valve → shell and tube heat exchanger → check valve 5 → liquid reservoir → dry filter → plate heat exchanger → electronic expansion valve 1 → outdoor finned tube heat exchanger → check valve 1 → four-way reversing valve → gas-liquid separator → compressor.

3. Cooling condition (i.e., defrosting condition): Solenoid valve 2 is closed, solenoid valve 1 is opened, electronic expansion valve 3 is electrified, and electronic expansion valves 1 and 2 are not electrified. Loop of the heat pump working fluid is compressor → four-way reversing valve → solenoid valve 1 → outdoor finned tube heat exchanger → check valve 2 → liquid reservoir → dry filter → plate heat exchanger → electronic expansion valve 3 → shell and tube heat exchanger → four-way reversing valve → gas-liquid separator → compressor. It should be noted that only the outdoor finned tube heat exchanger participates in this condition, while our design also allows the indoor finned tube heat exchanger to perform manual defrosting for special needs.

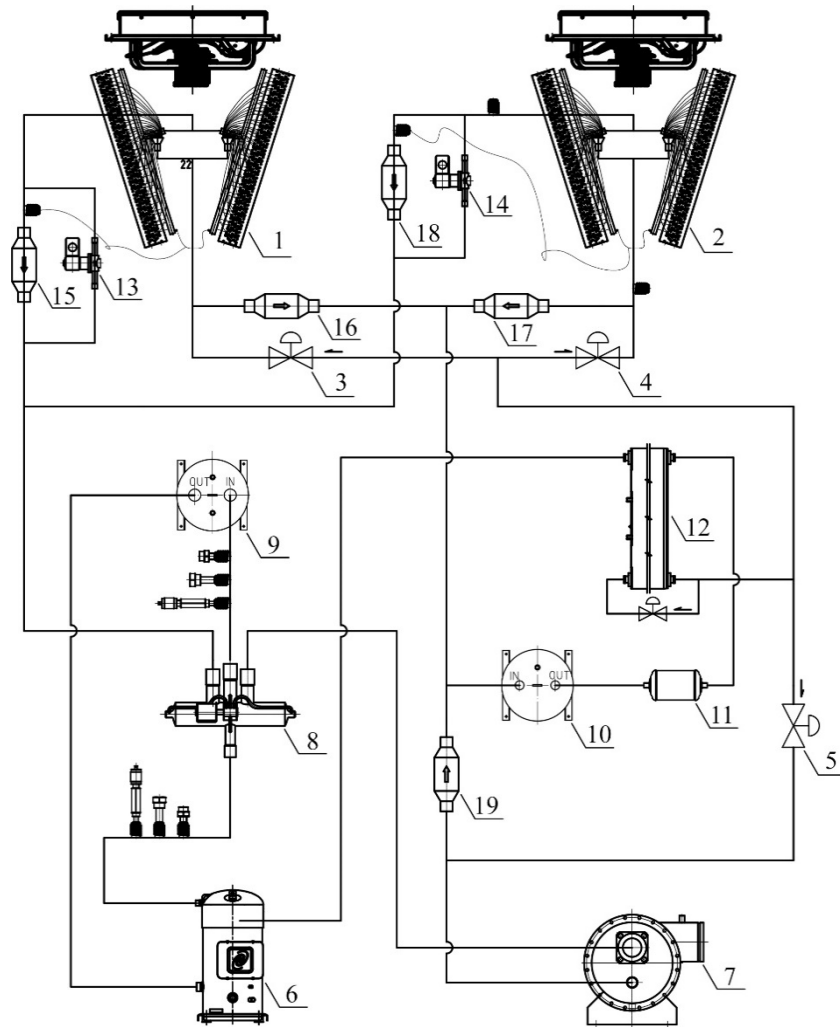
The heat storage tank stores CSG surplus air heat, collected by heat pumps during the day, and acts as the heat distribution center of the ETGHP system. Due to the higher outlet water temperature of the heat pump, the lower COP, and the higher operating cost [24, 45, 55], we recommended the maximum water temperature of the heat storage tank to be around 45 °C.

The heat release actuator circulates hot water, supplied by the heat storage tank, at temperatures that fluctuate in an extensive range (e.g., 25-45 °C). In this case, the frequently used radiators for greenhouse heating, such as rail pipes and finned pipes that work mainly through natural convection and thermal radiation, show no efficiency in heat release. Thus, forced-air convection equipment with a higher heat transfer coefficient is required [3]. The ETGHP system releases heat via parts of a combined air conditioning unit that includes functional sections of air inlet and filtration, evaporative cooling and humidification (wet pad), heating (surface air cooler), and fan and air outlet. Essentially, the air cooler is a water-air heat exchanger, usually using a finned tube type. These components are coordinated in a sequence, and functions of CO<sub>2</sub> supplement and ozone disinfection can also be added. The fan and surface air cooler are involved in greenhouse heating by internal air circulation. Such a design aims to integrate all components and controls to improve the cost-effectiveness of greenhouse climate management.

The ventilation duct comprises two parts, through which undesirable temperature gradients are

preventable. One part is connected to indoor fans of the dual source heat pump, enabling cold air after flowing through the indoor evaporator to be distributed uniformly to the CSG space. The second part is connected to the air outlet of the combined air conditioning unit, conveying heated air by surface air cooler to the cultivating area of the multi-span greenhouse. Two sets of water pumps and assorted circulating water pipes are installed on the heat pump and heat release sides.

Operation methods of the ETGHP system are as follows: 1) During winter daytime, the heat pump runs at the CSG air source condition and extracts surplus air heat inside the CSG. Then, the extracted heat energy, alongside the transformed energy from driving electricity, will be stored in the heat storage tank through water circulations. 2) If heat collection under CSG conditions fails to achieve temperature settings of the heat storage tank, e.g. on cloudy days or days experiencing extremely low temperatures, the heat pump continues to run with the outdoor air source heating condition for heat replenishment. 3) When air temperature inside the multi-span greenhouse drops to the setpoint, the combined air conditioning unit is turned on to release stored heat. 4) At night, when the water temperature of the heat storage tank decreases to the setpoint, the heat pump runs again with the outdoor condition to maintain temperatures within a specific range.



1. Outdoor finned tube heat exchanger 2. Indoor finned tube heat exchanger 3. Electronic expansion valve 1 4. Electronic expansion valve 2 5. Electronic expansion valve 3 6. Compressor 7. Shell and tube heat exchanger 8. Four-way reversing valve 9. Gas-liquid separator 10. Liquid reservoir 11. Dry filter 12. Plate heat exchanger 13. Solenoid valve 1 14. Solenoid valve 2 15. Check valve 1 16. Check valve 2 17. Check valve 3 18. Check valve 4 19. Check valve 5

Fig.2 Structural Diagram of the dual source heat pump

### 3. Calculation

Calculation processes for the ETGHP system sizing are shown in Fig. 3. These calculations are carried out on system and component levels. Therefore, configuring the components themselves (e.g., sizing the evaporators and condensers of the heat pump) is not within the research scope since this is generally the manufacturer's responsibility. In addition, sizing water pumps, circulating water pipes, and ventilation



commonly used for energy conservation, this model should be user-friendly for greenhouses with indoor thermal screens and an external thermal blanket. Also, it is expected to treat greenhouses cultivating fruiting and leafy vegetables differently to improve accuracy. Moreover, the complete reliability of the model should be valid for selecting the air source heat pump, which is sensitive to the ambient temperature variation.

Fu et al. [56] simplified the heating load model, only considering convective and conductive heat losses of greenhouse cover, as well as the heat loss due to air exchange. Simulation results showed that the heat loss through foundation walls accounted for roughly 0.1% of the total by the cover, and the heat loss through ground accounted for roughly 1% of the greenhouse heating load, both of which were not leading factors. However, Ahamed et al. [59] found that heat losses by conduction and convection, air infiltration, and long-wave radiation contributed 40%, 32%, and 21%, respectively. Furthermore, the proportion of radiative heat loss increased as the use of thermal screens was reduced. Heat loss experienced through long-wave radiation can therefore not be ignored.

According to Zhang et al. [62], when considering radiative heat transfer, heat loss through the greenhouse envelope can be estimated by calculating the heat transfer rate of the outermost cover layer or the heat transfer coefficient of the multi-layer cover. However, it will be overvalued since the model neglected the thermal resistance of each cover layer and air infiltration between layers, which is especially unsuitable for scenarios where cover layers have large thicknesses or high thermal resistances. Vanthoor et al. [63] developed a complex greenhouse climate model, establishing differential equations for indoor air, crops, floor, soil, thermal screen, the air above the thermal screen, and cover. This dynamic model assumed that internal and external cover surfaces each occupy 10% of the cover heat capacity, differing temperatures. The heating requirement can be obtained by returning differential equations to zero and analyzing heat transfer processes around indoor air at a steady state. These approaches have strong interpretability but are not directed to engineering design, especially for multi-span greenhouses with thermal insulation layers.

Thus, in this study, the heating load model takes indoor air and its inclusions as a whole object and analyzes related convection, conduction, and long-wave radiation processes. The heating load  $Q_h$  ( $\text{W m}^{-2}$ ) explicitly includes the combined heat transfer through envelope  $Q_{tr}$  ( $\text{W m}^{-2}$ ) and air infiltration heat loss  $Q_v$  ( $\text{W m}^{-2}$ ). It neglects heat losses through the indoor floor, foundation walls, and side walls below the horizontal plane (for a sunken greenhouse). The latent heat is also assumed to be negligible. In some cases, the maximum heating requirement occurs after uncovering thermal insulation layers rather than at

the lowest outdoor temperature. However, the time and the outdoor weather conditions for uncovering depends largely on growers, and is a challenging aspect to be estimated in engineering design. Furthermore, this period with potentially increased heating demand is short, owing to the increasing solar radiation entering the greenhouse [56]. This model, therefore, describes processes considering that greenhouses are covered and ignores the influences of solar radiation.

### 3.1.1. Model equations and parameterization

The multi-span greenhouse heating load  $Q_h$  is described by

$$Q_h = Q_{tr} + Q_v \quad (\text{W m}^{-2}) \quad (1)$$

In which,  $Q_{tr}$  is described by

$$Q_{tr} = \frac{1}{A_f} \sum (A_c U_c (\alpha_{ts} (1 - p_{ts}) + 1 - \alpha_{ts})) (t_a - t_g) \quad (\text{W m}^{-2}) \quad (2)$$

Where  $A_f$  ( $\text{m}^2$ ) is the greenhouse floor area;  $A_c$  ( $\text{m}^2$ ) is the greenhouse cover area, denoting the area of the roof, sidewall, or gutter with extensive area;  $p_{ts}$  (-) is the energy-saving fraction of the indoor thermal screen, which reflects reduction ratio to the heat transfer coefficient of the greenhouse cover [64]. Since energy-saving fraction has become the essential performance parameter of thermal screens, its use benefits simplified calculation.  $\alpha_{ts}$  (-) is a binary switch function, which is 1 when the indoor thermal screen is enabled and 0 when not enabled;  $t_g$  ( $^{\circ}\text{C}$ ) is the design temperature of greenhouse air;  $t_a$  ( $^{\circ}\text{C}$ ) is the design temperature of ambient air;  $U_c$  ( $\text{W m}^{-2} \text{ }^{\circ}\text{C}^{-1}$ ) is the overall heat transfer coefficient of the greenhouse cover, also known as effective heat transfer coefficient [3, 57], synthetically reflecting conduction, convection, and radiation processes. Since some transparent cover materials can transmit long-wave radiation, in this model,  $U_c$  considers not only the integrated heat transfer of indoor air and its inclusions to the outside by cover as usual [3], but also the radiative heat transfer between indoor radiating bodies and the sky directly passing through the cover. Generally, cover emissivity and transmittivity to long-wave radiation are trade-off parameters. That means when radiative heat loss caused by affecting cover temperatures is high, that caused by directly passing the cover would be low.

$U_c$  is expressed by

$$U_c = \left( \frac{1}{h_{c,in} + r_{c,in}^*} + \sum \frac{\delta_{c,i}}{\lambda_{c,i}} + \frac{1}{h_{c,out} + r_{c,out}^*} \right)^{-1} + r_{c,t}^* \quad (\text{W m}^{-2} \text{ }^{\circ}\text{C}^{-1}) \quad (3)$$

Where  $\lambda_{c,i}$  ( $\text{W m}^{-1} \text{ }^{\circ}\text{C}^{-1}$ ) is the thermal conductivity of each layer of greenhouse cover;  $\delta_{c,i}$  (m) is each layer thickness of the cover;  $h_{c,in}$  and  $h_{c,out}$  ( $\text{W m}^{-2} \text{ }^{\circ}\text{C}^{-1}$ ) are the convective heat transfer coefficients for

internal and external surfaces of cover, respectively;  $r_{c,in}^*$  ( $\text{W m}^{-2} \text{ }^\circ\text{C}^{-1}$ ) is the apparent radiation heat transfer coefficient between the internal surface of the cover and indoor radiating bodies. ‘Apparent’ indicates the actual object attending the radiative heat exchange is not air. However, this model takes indoor air and its inclusions as a whole radiating body, which means the indoor radiating bodies, such as crops, steel skeleton, and floor, have the same temperature as indoor air. Thus,  $r_{c,in}^*$  is also the actual coefficient.  $r_{c,out}^*$  ( $\text{W m}^{-2} \text{ }^\circ\text{C}^{-1}$ ) is the apparent radiation heat transfer coefficient between the external surface of the cover and the sky;  $r_{c,t}^*$  ( $\text{W m}^{-2} \text{ }^\circ\text{C}^{-1}$ ) is the apparent radiation heat transfer coefficient between the indoor radiating body and the sky through the cover.

$h_{c,in}$  and  $h_{c,out}$  can be estimated from the following empirical formulas [63, 65]:

$$h_{c,in} = \begin{cases} 2.21|t_g - t_{c,in}|^{0.33}, & \text{for plastic greenhouse} \\ 1.86|t_g - t_{c,in}|^{0.33}, & \text{for glass greenhouse} \end{cases} \quad (\text{W m}^{-2} \text{ }^\circ\text{C}^{-1}) \quad (4)$$

$$h_{c,out} = \begin{cases} 0.95 + 6.76v^{0.49}, & \text{for plastic greenhouse} \\ 7.2 + 3.84v, & \text{for glass greenhouse} \end{cases} \quad (\text{W m}^{-2} \text{ }^\circ\text{C}^{-1}) \quad (5)$$

Where  $t_{c,in}$  ( $^\circ\text{C}$ ) is the inner surface temperature of greenhouse cover;  $v$  ( $\text{m s}^{-1}$ ) is outdoor wind speed.

$r_{c,in}^*$  and  $r_{c,out}^*$  are calculated as follows:

$$r_{c,in}^* = \frac{\sigma \varepsilon_g \varepsilon_{c,in} A_g F_{g,c} ((t_g + 273.15)^4 - (t_{c,in} + 273.15)^4)}{A_c (t_g - t_{c,in})} \quad (\text{W m}^{-2} \text{ }^\circ\text{C}^{-1}) \quad (6)$$

$$r_{c,out}^* = \frac{\sigma \varepsilon_{c,out} \varepsilon_{sky} F_{c,sky} ((t_{c,out} + 273.15)^4 - (t_{sky} + 273.15)^4)}{t_{c,out} - t_a} \quad (\text{W m}^{-2} \text{ }^\circ\text{C}^{-1}) \quad (7)$$

Where  $\sigma = 5.67 \times 10^{-8} \text{ W m}^{-2} \text{ K}^{-4}$  is the Stefan-Boltzmann constant;  $\varepsilon_g = 1$  is the emissivity of the indoor radiating body [63, 66];  $\varepsilon_{c,in}$  (-) and  $\varepsilon_{c,out}$  (-) are the emissivity of internal and external surfaces of greenhouse cover, respectively. The emissivity is 0.85 for glass cover [63], 0.15 for polyethylene (PE) film [62], 0.62 for polyvinyl chloride (PVC) film, and 0.59 for ethyl vinyl acetate (EVA) film [67].  $\varepsilon_{sky} = 1$  is sky emissivity [62, 63];  $A_g$  ( $\text{m}^2$ ) is the total surface area of indoor radiating bodies, that is, the surface area of the whole radiating body;  $F_{g,c}$  (-) is the view factor of indoor radiating body to the internal surface of the cover;  $F_{c,sky} = 1$  is the view factor of the external surface of the cover to the sky, ignoring radiation heat exchange with outdoor ground [62];  $t_{c,out}$  ( $^\circ\text{C}$ ) is the outer surface temperature of the cover;  $t_{sky}$  ( $^\circ\text{C}$ ) is the effective sky temperature.

In modern multi-span greenhouses, steel skeletons are intensive, and crop density can be very high. Moreover, cultivated fruiting vegetables can grow very tall (e.g., tomato), benefiting from the tendril hanging. So it is insufficient to determine radiative heat exchanges of the indoor radiating body using

floor area, especially for small-scale greenhouses. The indoor radiating body is assumed to be a pentahedron for multi-span greenhouses planting fruiting vegetables, and  $A_g$  can be calculated by

$$A_g = A_f + peH_g \quad (\text{m}^2) \quad (8)$$

Where  $pe$  (m) is the greenhouse perimeter, and  $H_g$  (m) is the height of greenhouse sidewalls excluding foundation walls.

To greenhouse roof,  $F_{g,c}$  is calculated by

$$F_{g,c} = \frac{A_f}{A_g} \quad (-) \quad (9)$$

If the gutter area cannot be neglected,  $F_{g,c}$  for gutter will share  $A_f/A_g$  with the roof in proportion to their horizontal projection areas.

According to the completeness of view factor,  $F_{g,c}$  to greenhouse sidewalls is estimated by

$$F_{g,c} = \frac{peH_g}{A_g} \quad (-) \quad (10)$$

For greenhouses cultivating leaf vegetables,  $A_g = A_f$ . Then to greenhouse roof,  $F_{g,c}$  is calculated by the following formula [68]:

$$F_{g,c} = \frac{2H_g^2}{\pi A_f} \left( \ln \left( \frac{\left(1 + \left(\frac{W}{H_g}\right)^2\right) \left(1 + \left(\frac{L}{H_g}\right)^2\right)}{1 + \left(\frac{W}{H_g}\right)^2 + \left(\frac{L}{H_g}\right)^2} \right)^{\frac{1}{2}} + \frac{W}{H_g} \left(1 + \left(\frac{L}{H_g}\right)^2\right)^{\frac{1}{2}} \operatorname{atan} \frac{\frac{W}{H_g}}{\left(1 + \left(\frac{L}{H_g}\right)^2\right)^{\frac{1}{2}}} + \frac{L}{H_g} \left(1 + \left(\frac{W}{H_g}\right)^2\right)^{\frac{1}{2}} \operatorname{atan} \frac{\frac{L}{H_g}}{\left(1 + \left(\frac{W}{H_g}\right)^2\right)^{\frac{1}{2}}} - \frac{W}{H_g} \operatorname{atan} \frac{W}{H_g} - \frac{L}{H_g} \operatorname{atan} \frac{L}{H_g} \right) \quad (-) \quad (11)$$

Where  $L$  (m) is the greenhouse length;  $W$  (m) is the greenhouse width. The calculation of view factors of the indoor radiating body to gutter and sidewalls refers to the rules used by the fruiting vegetable greenhouse.

On sunny days,  $t_{sky}$  is obtained from the following formula [67]:

$$t_{sky} = 0.0552(t_a + 273.15)^{1.5} - 273.15 \quad (^\circ\text{C}) \quad (12)$$

$t_{c,in}$  ( $^\circ\text{C}$ ) and  $t_{c,out}$  are determined by solving the following heat balance equations of greenhouse cover.

Then, parameters of  $h_{c,in}$ ,  $h_{c,out}$ ,  $r_{c,in}^*$ , and  $r_{c,out}^*$  can be obtained.

$$\begin{cases} (h_{c,in} + r_{c,in}^*)(t_g - t_{c,in}) = \left(\sum \frac{\delta_{c,i}}{\lambda_{c,i}}\right)^{-1} (t_{c,in} - t_{c,out}) \\ (h_{c,out} + r_{c,out}^*)(t_{c,out} - t_a) = \left(\sum \frac{\delta_{c,i}}{\lambda_{c,i}}\right)^{-1} (t_{c,in} - t_{c,out}) \end{cases} \quad (\text{W m}^{-2}) \quad (13)$$

$r_{c,t}^*$  is calculated by

$$r_{c,t}^* = \frac{\sigma \varepsilon_g \varepsilon_{sky} A_g F_{g,c} \tau_c ((t_g + 273.15)^4 - (t_{sky} + 273.15)^4)}{A_c (t_g - t_a)} \quad (\text{W m}^{-2} \text{ } ^\circ\text{C}^{-1}) \quad (14)$$

Where  $\tau_c$  (-) is the transmittance of greenhouse cover to long-wave radiation, which is 0 for glass [62, 63], 0.75 for PE film [62], 0.33 for PVC film, and 0.38 for EVA film [67]. For a multi-layer greenhouse cover,  $\tau_c$  is the product of transmittances of each layer of materials.

$Q_v$  is described as follows [69]:

$$Q_v = g_{v,leak} \rho_{air} c_{p,air} (t_g - t_a) \quad (\text{W m}^{-2}) \quad (15)$$

$$g_{v,leak} = \frac{NH}{3600} \quad (\text{m s}^{-1}) \quad (16)$$

Where  $g_{v,leak}$  ( $\text{m s}^{-1}$ ) is the specific ventilation rate of greenhouse due to air infiltration;  $\rho_{air} = 1.3 \text{ kg m}^{-3}$  is the air density;  $c_{p,air} = 1,006 \text{ J kg}^{-1} \text{ } ^\circ\text{C}^{-1}$  is the specific heat of air at constant pressure;  $N = 1 \text{ h}^{-1}$  is the infiltration rate [56, 59];  $H$  (m) is the greenhouse average height, taking indoor floor as the benchmark.

When the greenhouse adopts two or more layers of indoor thermal screens,  $p_{ts}$  is calculated by the following formula [70]:

$$p_{ts} = \frac{\sum \frac{p_{ts,i}}{1-p_{ts,i}}}{1 + \sum \frac{p_{ts,i}}{1-p_{ts,i}}} \quad (-) \quad (17)$$

Where  $p_{ts,i}$  (-) is the energy-saving fraction by each layer of the indoor thermal screen.

When the multi-span greenhouse adopts an external thermal blanket, which is commonly closely attached to the outer surfaces of the greenhouse cover (e.g., roof), the blanket can be regarded as a component of the cover constituted by multi-layer materials. Correspondingly, the infiltration rate  $N$  is halved to  $0.5 \text{ h}^{-1}$  [71] because some cracks become sealed in the greenhouse covering. Then, the usage of the energy-saving fraction depends upon the installation of indoor thermal screens. Another difference is that materials of the external thermal blanket, instead of the roof, will determine the emissivity of the cover's outer surface ( $\varepsilon_{c,out}$ ). The convective heat transfer coefficient for the cover's outer surface ( $h_{c,out}$ ) refers to Eqs (5) yet.

### 3.1.2. Definition of design temperatures

The specific design temperatures of indoor and outdoor air are commonly defined in greenhouse heating load calculations. For the design outdoor air temperature, the average of annual minimum temperatures over the past 20-30 years can be used [48, 61], or it should meet a certain proportion (e.g., 99.5%) of heating requirements in a long term [3]. However, these methods are not transparent enough that indoor temperatures cannot be determined under extremely low-temperature conditions. It is risky to make heating equipment selections according to such methods, especially for the air source heat pump, of which the heating capacity will decrease as ambient air temperature decreases [13, 24, 55].

This study puts forward a hierarchical valuing method for the design temperatures of indoor and outdoor air. The first is to count local outdoor air temperatures (time interval  $\leq 1$  h) across the heating seasons and arrange them in ascending order. Thus, as the design outdoor air temperature ( $t_a$ ) takes the 10<sup>th</sup> percentile  $t_{a,1}$  and the design indoor air temperature ( $t_g$ ) takes  $t_{g,1}$ , the guaranteed rate for indoor air temperature  $\geq t_{g,1}$  is 90%. Analogously, as  $t_a$  takes the 5<sup>th</sup> percentile  $t_{a,2}$  and  $t_g$  takes  $t_{g,2}$ , the guaranteed rate of indoor air temperature  $\geq t_{g,2}$  is 95%. As  $t_a$  takes the lowest  $t_{a,3}$  and  $t_g$  takes  $t_{g,3}$ , the guaranteed rate of indoor air temperature  $\geq t_{g,3}$  is 100%. Then the greenhouse heating load takes the highest value from the three situations. This hierarchical valuing method can locate the lower limit of greenhouse air temperature, ensuring that crops never encounter freezing injury under extreme weather. This method can also help avoid installed capacity excess of the heating equipment. Meanwhile, according to the principle of temperature integration [72], short-term low temperatures caused by this method would not impede crop growth. Taking the weather data of Shouguang, Shandong Province, China during the winter season of 2020-2021 as an example (Fig. 4), design temperatures of indoor and outdoor air, for a multi-span greenhouse planting tomatoes, are shown in Table 1.

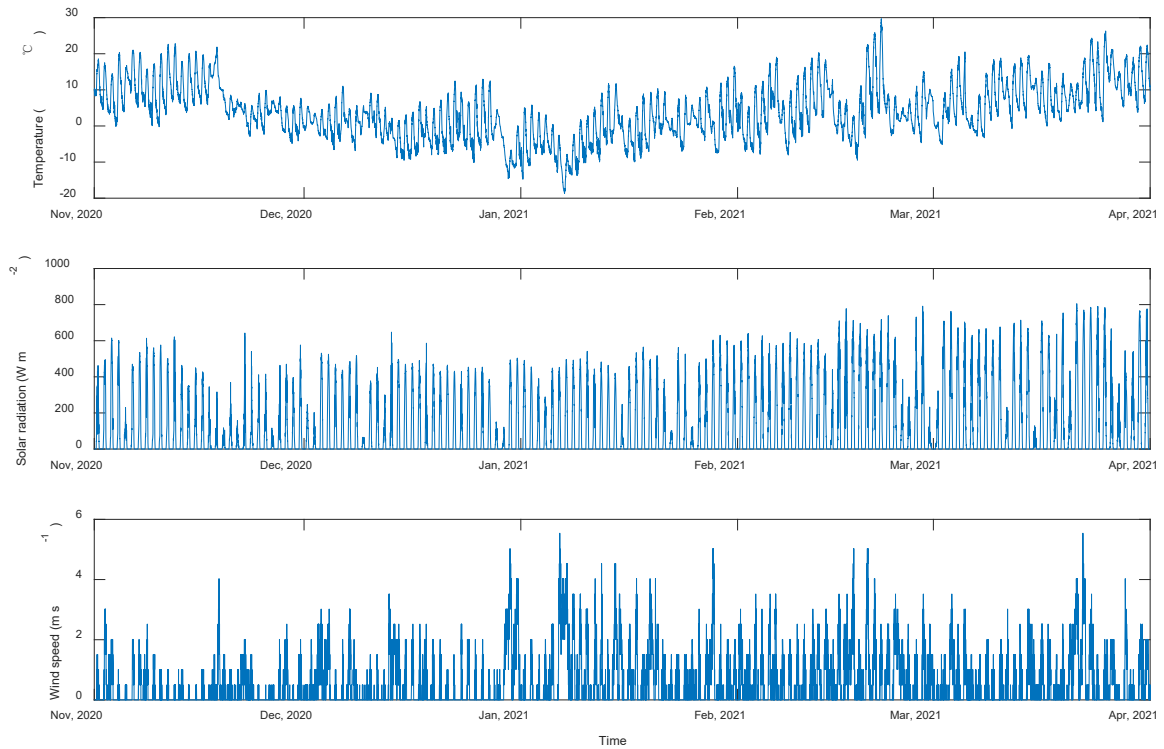


Fig. 4 Ambient air temperature, solar radiation, and wind speed during greenhouse heating seasons in Shouguang, Shandong Province, China (2020-2021)

Table 1 Design temperatures using the hierarchical valuing method for calculating heating load of a multi-span greenhouse cultivating tomatoes based on weather data in Fig. 4

Design indoor air temperature $t_g$ (°C)	Guaranteed rate of indoor air temperature $\geq t_g$ (%)	Design outdoor air temperature $t_a$ (°C)
18	90	-5.5
14	95	-7.4
10	100	-18.7

### 3.2. Surplus air heat model of CSGs

Quantification of surplus air heat inside CSGs is the basis of sizing the equipment utilizing surplus air heat, optimizing climate control strategies, and improving the greenhouse heat energy using efficiency. The surplus air heat model of CSGs should take indoor air, where the ETGHP system directly draws heat, as the analysis object, studying heat fluxes flowing to indoor air that make the air temperature higher than the reference. It is similar to modeling the greenhouse cooling demand [26]. Therefore, this model is

developed based on the foundation framework of the CSG cooling load model by Sun et al. [69].

### 3.2.1. Model equations and parameterization

Heat transfer processes contributing to the generation of CSG surplus air heat include convections between indoor air and internal surfaces of the north wall ( $Q_{nw}$ ), north roof ( $Q_{nr}$ ), transparent south roof ( $Q_{sr}$ ), and indoor floor ( $Q_{fc}$ ), as well as air exchange ( $Q_{vc}$ ). Heat transfer processes of sidewalls are neglected. The CSG surplus air heat ( $Q_s$ ) can be calculated by the following formulas:

$$Q_s = Q_{nw} + Q_{nr} + Q_{fc} - Q_{sr} - Q_{vc} \quad (\text{W m}^{-2}) \quad (18)$$

$$\begin{bmatrix} Q_{nw} \\ Q_{nr} \\ Q_{fc} \\ Q_{sr} \end{bmatrix} = \frac{1}{A_{fc}} \begin{bmatrix} A_{nw} CVH_{nw,in\_gC} \\ A_{nr} CVH_{nr,in\_gC} \\ A_{fc} CVH_{fc\_gC} \\ A_{sr} CVH_{gC\_sr,in} \end{bmatrix} = \frac{1}{A_{fc}} \begin{bmatrix} A_{nw} h_{nw,in} (t_{nw,in} - t_{gC}) \\ A_{nr} h_{nr,in} (t_{nr,in} - t_{gC}) \\ A_{fc} h_{fc} (t_{fc} - t_{gC}) \\ A_{sr} h_{sr,in} (t_{gC} - t_{sr,in}) \end{bmatrix} \quad (\text{W m}^{-2}) \quad (19)$$

Convective heat transfer coefficients in Eqs. (19) can be given by empirical formulas [65]. Therefore, the critical point of the model is to obtain temperatures of internal surfaces of the CSG envelope and indoor floor. Since the effects of thermal radiation were not considered, simulated temperatures of internal surfaces of the north wall and indoor floor are excessively high in line with Sun et al. [69]. In this model, radiative heat transfers from internal surfaces of the north wall, north roof, and indoor floor to the transparent south roof and the sky through the south roof are involved. In addition, the north roof angle of the CSG is currently designed to be 42-50° that the north roof could receive as much solar radiation [73]. Therefore, besides the north wall and indoor floor, the solar radiation received by the north roof should be considered.

For simplification, radiative heat exchanges among the north wall, north roof, and indoor floor are assumed to be negligible. The north wall and north roof have considerable thermal resistances, and the radiation heat transfer of their external surfaces contributes very little to heat fluxes from their internal surfaces to the outside. To avoid solving the two external surface temperatures and decrease the number of simultaneous equations, the radiative effects of the two external surfaces are ignored. Thus, a comprehensive coefficient considering convection and conduction can be adopted. Conversely, the transparent south roof has small thermal resistance, and radiative processes largely affect its heat transfer coefficient and the internal surface temperature. The one-through heat transfer coefficient, only considering convection and conduction, is therefore no longer applicable. On the one hand, the south roof internal surface should consider radiation heat exchanges with the north wall, north roof, and indoor floor.

On the other hand, its external surface should consider radiation heat exchange with the sky, ignoring interactions with the ground.

Heat balance equations of the north wall internal surface are described as follows:

$$I_{nw,in}\alpha_{nw,in} = CVH_{nw,in\_gC} + CTH_{nw,in\_a} + RSH_{nw,in\_sr,in} + RTH_{nw,in\_sky} \quad (\text{W m}^{-2}) \quad (20)$$

$$CTH_{nw,in\_a} = k_{nw}(t_{nw,in} - t_a) \quad (\text{W m}^{-2}) \quad (21)$$

$$RSH_{nw,in\_sr,in} = \sigma\varepsilon_{nw,in}\varepsilon_{sr,in}F_{nw,sr} \left( (t_{nw,in} + 273.15)^4 - (t_{sr,in} + 273.15)^4 \right) \quad (\text{W m}^{-2}) \quad (22)$$

$$RTH_{nw,in\_sky} = \sigma\varepsilon_{nw,in}\varepsilon_{sky}F_{nw,sr}\tau_{sr} \left( (t_{nw,in} + 273.15)^4 - (t_{sky} + 273.15)^4 \right) \quad (\text{W m}^{-2}) \quad (23)$$

$$k_{nw} = \left( \frac{1}{h_{nw,out}} + \sum \frac{\delta_{nw,i}}{\lambda_{nw,i}} \right)^{-1} \quad (\text{W m}^{-2} \text{ } ^\circ\text{C}^{-1}) \quad (24)$$

$$h_{nw,out} = 7.2 + 3.84v \quad (\text{W m}^{-2} \text{ } ^\circ\text{C}^{-1}) \quad (25)$$

$$h_{nw,in} = 3.4|t_{nw,in} - t_{gC}|^{0.33} \quad (\text{W m}^{-2} \text{ } ^\circ\text{C}^{-1}) \quad (26)$$

Where  $k_{nw}$  ( $\text{W m}^{-2} \text{ } ^\circ\text{C}^{-1}$ ) is the comprehensive heat transfer coefficient between the internal surface of the north wall and outdoor air.

Heat transfer processes of the north roof internal surface and relevant parameters are similar to those of the north wall. Thus, only the central heat balance equation is listed here.

$$I_{nr,in}\alpha_{nr,in} = CVH_{nr,in\_gC} + CTH_{nr,in\_a} + RSH_{nr,in\_sr,in} + RTH_{nr,in\_sky} \quad (\text{W m}^{-2}) \quad (27)$$

Heat balance equations of the indoor floor are as follows:

$$I_{fC}\alpha_{fC} = CVH_{fC\_gC} + CDH_{fC\_cs} + RSH_{fC\_sr,in} + RTH_{fC\_sky} \quad (\text{W m}^{-2}) \quad (28)$$

$$CDH_{fC\_cs} = \frac{\lambda_{soil}}{\delta_{cs}}(t_{fC} - t_{cs}) \quad (\text{W m}^{-2}) \quad (29)$$

$$h_{fC} = 5.2|t_{fC} - t_{gC}|^{0.33} \quad (\text{W m}^{-2} \text{ } ^\circ\text{C}^{-1}) \quad (30)$$

Where  $\lambda_{soil} = 0.83 \text{ W m}^{-1} \text{ } ^\circ\text{C}^{-1}$  is the thermal conductivity of soil;  $\delta_{cs} = 3 \text{ m}$  is the soil depth of constant temperature;  $t_{cs} = 15 \text{ } ^\circ\text{C}$  is the constant soil temperature. Expressions of  $RSH_{fC\_sr,in}$  and  $RTH_{fC\_sky}$  can refer to Eqs. (22) and (23).

Heat balance equations of the south roof are as follows:

$$A_{sr}CVH_{gC\_sr,in} + A_{nw}RSH_{nw,in\_sr,in} + A_{nr}RSH_{nr,in\_sr,in} + A_{fC}RSH_{fC\_sr,in} = A_{sr}CDH_{sr,in\_sr,out} \quad (\text{W m}^{-2}) \quad (31)$$

$$CVH_{sr,out\_a} + RTH_{sr,out\_sky} = CDH_{sr,in\_sr,out} \quad (\text{W m}^{-2}) \quad (32)$$

$$CVH_{sr,out\_a} = h_{sr,out}(t_{sr,out} - t_a) \quad (\text{W m}^{-2}) \quad (33)$$

$$RTH_{sr,out\_sky} = \sigma \varepsilon_{sr,out} \varepsilon_{sky} F_{sr,sky} \left( (t_{sr,out} + 273.15)^4 - (t_{sky} + 273.15)^4 \right) \quad (\text{W m}^{-2}) \quad (34)$$

$$CDH_{sr,in\_sr,out} = \left( \sum \frac{\delta_{sr,i}}{\lambda_{sr,i}} \right)^{-1} (t_{sr,in} - t_{sr,out}) \quad (\text{W m}^{-2}) \quad (35)$$

$$h_{sr,in} = 7.2 + 3.84 v_{gC} \quad (\text{W m}^{-2} \text{ } ^\circ\text{C}^{-1}) \quad (36)$$

Where  $v_{gC} = 1 \text{ m s}^{-1}$  is the indoor wind speed caused by air circulation to collect the CSG surplus air heat. The calculation of  $h_{sr,out}$  can refer to Eqs. (25).

The temperatures of internal surfaces of the north wall, north roof, south roof, and indoor floor are determined by solving simultaneous equations of Eqs. (20), (27), (28), and (31).

Since the CSG extends in the east-west direction and side walls have been ignored in the model description, the radiant energy emitted to the east and west ends can be omitted. Then the CSG cross-section is considered as a closed system. According to dimensions of the CSG cross-section (Fig. 5), view factors between different surfaces are estimated as follows based on the algebraic analysis method [47]:

$$F_{nw, sr} = \frac{L_{cl1} + L_{cl2} - L_{fC} - L_{nr}}{2L_{nw}} \quad (-) \quad (37)$$

$$F_{nr, sr} = \frac{L_{nr} + L_{sr} - L_{cl2}}{2L_{nr}} \quad (-) \quad (38)$$

$$F_{fC, sr} = \frac{L_{fC} + L_{sr} - L_{cl1}}{2L_{fC}} \quad (-) \quad (39)$$

Where  $L_{fC}$ ,  $L_{nw}$ ,  $L_{nr}$ , and  $L_{sr}$  (m) are the CSG span, height of the north wall, width of the north roof, and arc length of the south roof, respectively;  $L_{cl1}$  (m) is the length of connecting line between the roof ridge and the bottom angle of the north wall, and  $L_{cl2}$  (m) is the length of connecting line between the bottom angle of the south roof and the apex of the north wall.

The model does not distinguish between direct and scattered radiations. The indoor floor and internal surfaces of the north roof and north wall wholly or partially receive solar radiation following solar altitude variation. Thus, the solar energy received by them are respectively calculated by

$$I_{fC} = \zeta I_{f,out} \min \left[ 1, \frac{H_{rid} \cot \theta_{sun} + H_{rid} \cot \theta_{sr}}{L_{fC}} \right] \quad (\text{W m}^{-2}) \quad (40)$$

$$I_{nr,in} = \zeta I_{f,out} \max \left[ \frac{(H_{rid} \cot \theta_{sun} + H_{rid} \cot \theta_{sr} - L_{fC}) \sin(\theta_{nr} - \theta_{sun})}{L_{cl1} \sin(\theta_{nw} - \theta_{sun} - \theta_{cl1})}, 0 \right] \quad (\text{W m}^{-2}) \quad (41)$$

$$I_{nw,in} = \frac{\zeta I_{f,out}}{L_{nw}} \min \left[ 1 - \frac{L_{nr} \sin(\theta_{nr} - \theta_{sun})}{L_{cl1} \sin(\theta_{nw} - \theta_{sun} - \theta_{cl1})}, 1 \right] (H_{rid} \cot \theta_{sun} + H_{rid} \cot \theta_{sr} - L_{fC}) \quad (\text{W m}^{-2}) \quad (42)$$

Where  $H_{rid}$  (m) is the ridge height of the CSG;  $\theta_{sun}$  ( $^\circ$ ) is the solar altitude;  $\theta_{nw}$  ( $^\circ$ ) is the angle between the north wall and floor;  $\theta_{nr}$  ( $^\circ$ ) is the angle of the north roof;  $\theta_{sr}$  ( $^\circ$ ) is the angle of the south roof;  $\theta_{cl1}$  ( $^\circ$ ) is the angle between  $L_{cl1}$  and the north wall;  $I_{f,out}$  ( $\text{W m}^{-2}$ ) is the outdoor solar radiation in the horizontal

direction;  $\zeta (-)$  is the total transmittance of the south roof to solar radiation, it can be taken as 0.78 when the external shading screen and thermal blanket are not covered [74]. See Fig. 5,  $L_{cl1}$ ,  $L_{cl2}$ , and  $\theta_{cl1}$  are fixed values for a given CSG. These model inputs can be obtained by measurement, drawing software, or calculation based on the cosine theorem.

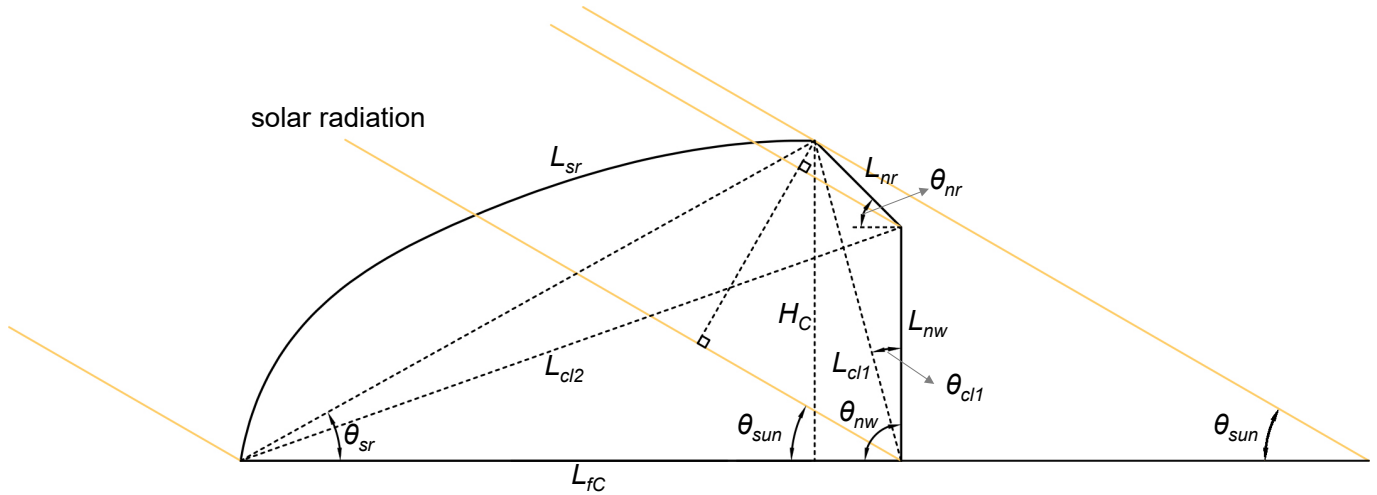


Fig. 5 CSG cross-section dimensions for calculations of view factors and received solar radiation

Greenhouse growers usually open roof vents to prevent excess heat, decrease humidity [31], and supplement CO<sub>2</sub>. However, excess heat and humidity are not always avoidable, even if the equipment utilizing surplus air heat is used, especially when CSGs are not uniformly managed. Therefore, the heat transfer by air exchange  $Q_{vC}$  comprehensively considers air infiltration and natural ventilation [75]:

$$Q_{vC} = \left( \frac{N_C H_C}{3600} + g_{v,roof} \right) \rho_{air} c_{p,air} (t_{gC} - t_a) \quad (\text{W m}^{-2}) \quad (43)$$

$$g_{v,roof} = \frac{0.81 L_v^{1.5} \left( \frac{t_{gC} - t_a}{t_a} \right)^{0.5} + 0.078 L_v v}{L_{fC}} \quad (\text{m s}^{-1}) \quad (44)$$

Where  $N_C$  ( $\text{h}^{-1}$ ) is the infiltration rate of the CSG;  $g_{v,roof}$  ( $\text{m s}^{-1}$ ) is the specific ventilation rate of the CSG due to roof ventilation;  $L_v = 0.15$  m is a given open width of roof vents;  $H_C$  (m) is the average height of the CSG based on the indoor floor.

### 3.2.2. Definition of design climate factors

The design CSG air temperature ( $t_{gC}$ ), that is the reference temperature generating surplus air heat, depends on the cultivated crop (e.g., 28 °C for tomatoes and 25 °C for lettuce). The model should reasonably select design values of outdoor climate factors to avoid excessive installed capacity and

prevent equipment from frequently switching on-off. This will ensure the high use efficiency of surplus air heat during the heating season and improve overall heating performance. It is recommended to count outdoor air temperature, solar radiation, and wind speed (time interval  $\leq 1$  h) from 10:00 to 15:00 in ascending order and take the 7<sup>th</sup>, 7<sup>th</sup>, and 3<sup>rd</sup> decile, respectively. As a result, the CSG surplus air heat will be fully utilized more than 70% of the time. The installed equipment runs at maximum capacity during rest periods, taking CSG surplus air heat as the heat source. For the given solar radiation, the north wall or north roof receives more solar radiation as the solar altitude decreases. The model takes the 7<sup>th</sup> decile of the solar altitude data from 10:00 to 15:00 over the heating season, since the variation trend of solar altitude is roughly similar to solar radiation. Variation of the solar altitude can be calculated by referring to [76]. Using the weather data of Shouguang in the winter of 2020-2021 (Fig. 4) as an example, the model inputs of design outdoor air temperature, solar radiation, solar altitude, and wind speed for equipment selection are 13.5°C, 480.6 W m<sup>-2</sup>, 36°, and 0.5 m s<sup>-1</sup>, respectively.

### 3.3. Dimensioning the key equipment

#### 3.3.1. Heat pump

The CSG surplus air heat is unstable due to greenhouse management and outdoor influencing weather changes, e.g. it cannot serve as the heat source on cloudy days and during extremely low-temperature weather conditions. First, the heating capacity of the heat pump taking ambient air as the heat source should meet the heating load of multi-span greenhouses. Its rated capacity  $HP_{a,rc}$  (W) is calculated by

$$HP_{a,rc} = \beta_{hp} \frac{COP_{rc} E_{rc}}{COP_{ta} E_{ta}} \sum Q_h A_f \quad (\text{W}) \quad (45)$$

Where  $COP_{rc}$  (-) and  $E_{rc}$  (W) are the heating COP and input electric power of the air source heat pump under the rated condition, respectively, both are factory parameters. For COP calculation, power-consuming components include compressors and fans, excluding circulating water pumps (the same below).  $COP_{ta}$  (-) and  $E_{ta}$  (W) are the heating COP value and input electric power at the outdoor air temperature of  $t_a$  and the outlet water temperature of 40-50°C, respectively;  $\beta_{hp}$  (-) is the extra coefficient, which is generally not more than 1.2. It must be emphasized that, when the air source heat pump is used as the single source or to provide a guarantee for greenhouse heating, its selection should meet the heating requirements under all the design temperature combinations. Hence, if the greenhouse heating load is not obtained at the lowest design outdoor air temperature, it will probably not determine the heat pump selection.

If measured data are not available, the COP and the input power of the air source heat pump under different working conditions can be estimated referring to the fitting functions in Fig. 6. According to  $HP_{a,rc}$  and the capacity of a single heat pump module, the number of required modules and the installed capacity of the air source heat pump  $HP_{a,ins}$  (W) are determined.

Then, the rated capacity of heat pump modules that adopt double sources  $HP_{d,rc}$  (W) is determined by the following formula:

$$HP_{d,rc} = \min\left(\frac{COP_{rc}}{COP_{gC}-1} \sum Q_s A_{fC}, HP_{a,ins}, \frac{TD_g \sum Q_h A_f}{TD_{gC}}\right) \text{ (W)} \quad (46)$$

Where  $COP_{gC} = 4.5$  is the COP of the heat pump taking CSG surplus air heat as the heat source, not considering the power consumption of water pumps [46];  $TD_{gC} = 5$  h is assigned running time of the heat pump under CSG air source heating condition [34, 36, 37], and  $TD_g = 13$  h is assigned time duration for heating the multi-span greenhouse in a 24-hour cycle. This formula ignores the difference of heat pump input powers between the rated and the CSG air source conditions due to the lack of data (the same below). According to  $HP_{d,rc}$  and the module capacity, the installed capacity of the dual source heat pump  $HP_{d,ins}$  (W) is determined.

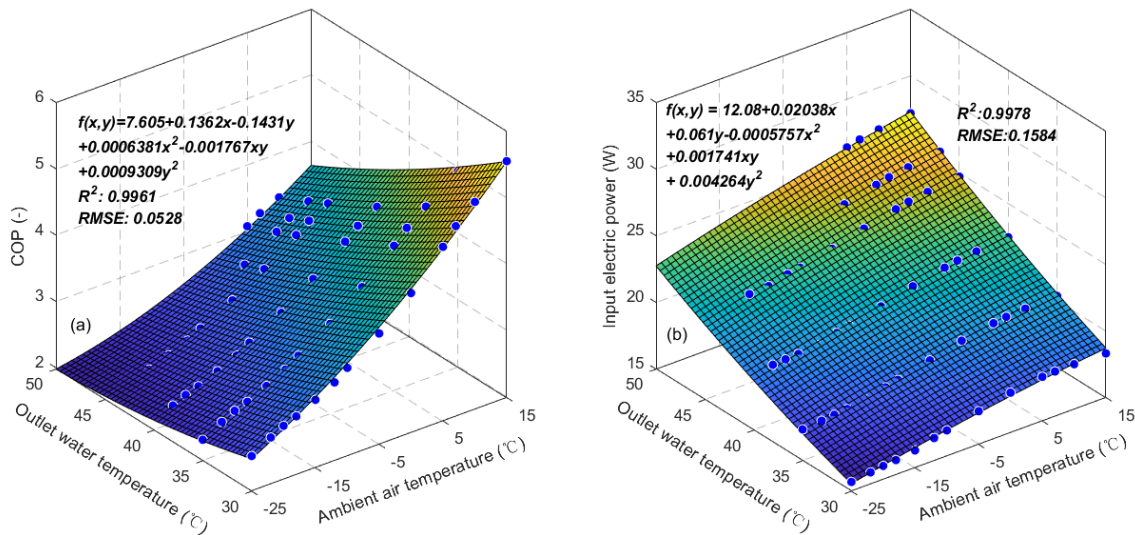


Fig. 6 Effects of outdoor air temperature (x-axis) and outlet water temperature (y-axis) on the heating COP (a) and input electric power (b) of the heat pump. The fitting functions are specific to a heat pump module with a rated electric power of 24.2 kW and COP of 3.55 under an ambient temperature of 7°C and an outlet water temperature of 45°C.

### 3.3.2. Heat storage tank

The effective volume of the heat storage tank  $V_{tank}$  (m<sup>3</sup>) should match the heating capacity of the dual source heat pump under CSG air source heating conditions. Meanwhile, it is recommended to stay within the heating demands of multi-span greenhouses in a 24-hour heating cycle. Thus,  $V_{tank}$  can be estimated by

$$V_{tank} = \min \left( \frac{3600 \times TD_g \times HP_{d,ins} \times \frac{COP_{gc}}{COP_{rc}}}{c_{p,w} \rho_w \Delta t_{tank}}, \frac{3600 \times TD_g \sum Q_h A_f}{c_{p,w} \rho_w \Delta t_{tank}} \right) \quad (\text{m}^3) \quad (47)$$

Where  $c_{p,w} = 4200 \text{ J kg}^{-1} \text{ }^\circ\text{C}^{-1}$  is the specific heat of water at constant pressure, ignoring the influence of water temperature;  $\rho_w = 1000 \text{ kg m}^{-3}$  is the density of water;  $\Delta t_{tank}$  ( $^\circ\text{C}$ ) is the temperature difference of the heat storage tank. The water temperature of the heat storage tank generally fluctuates from 25 to 45  $^\circ\text{C}$  when greenhouses are heated by air-water heat exchangers. Thus,  $\Delta t_{tank}$  takes the value of 20  $^\circ\text{C}$ .

### 3.3.3. Surface air cooler

The rated heat release capacity of the surface air cooler  $SAC$  (W) is calculated by

$$SAC = \beta_{sac} \sum Q_h A_f \quad (\text{W}) \quad (48)$$

Where  $\beta_{sac}$  (-) is the correction coefficient for surface air cooler selection, only considering effects of face velocity on heat exchange rate. The fan that works together with the surface air cooler is designed to meet demands for ventilation and evaporative cooling in summer, which is not within the scope of this study. However, the rated capacity of the surface air cooler is usually defined at face velocities ranging from 2 to 3  $\text{m s}^{-1}$  with a fan output frequency of 50 Hz. The ETGHP system adopts internal air circulation for heating in winter. For energy saving, it is recommended that the fan frequency would not be higher than 40 Hz in practice since the discharge air volume is reduced by 20% as the frequency decreases from 50 to 40 Hz, while power consumption is reduced by 48.8%. At the same time, the installed capacity of the surface air cooler should be increased to compensate for the shortage of heat exchange rate caused by the face velocity reduction. Thus,  $\beta_{sac}$  approximates 1.17 with integrated consideration that reducing face velocity improves the heat exchange efficiency.

### 3.3.4. Area Matching

The above calculations for equipment selection are based on the premise that the available area of CSGs is known. When greenhouses are designed to be built specifically for the application of the ETGHP system (or the available CSG area is known to be large enough and it is necessary to determine the

selected area), the area matching between multi-span greenhouses and CSGs is proposed as

$$\sum Q_s A_{fC} \geq \min \left( HP_{a,ins} \frac{COP_{gC}-1}{COP_{rc}}, \frac{TD_g \sum Q_h A_f}{TD_{gC}} \right) \text{ (W)} \quad (49)$$

## 4. Results and discussion

### 4.1. System implementation

According to the system design framework illustrated in Section 2 and Section 3, the ETGHP system was built in Shouguang city, Shandong province, China (36° 54' N, 118° 51' E). It extracted surplus air heat from six CSGs to heat a multi-span greenhouse, a CSG for seedling production, and an equipment room (Fig. 7). The system consisted of dual source heat pump units, a heat storage tank, fans and surface air coolers, water pumps, ventilating ducts, circulating water pipes, and a control system. Fig. 8 presents images of the main components of the system.

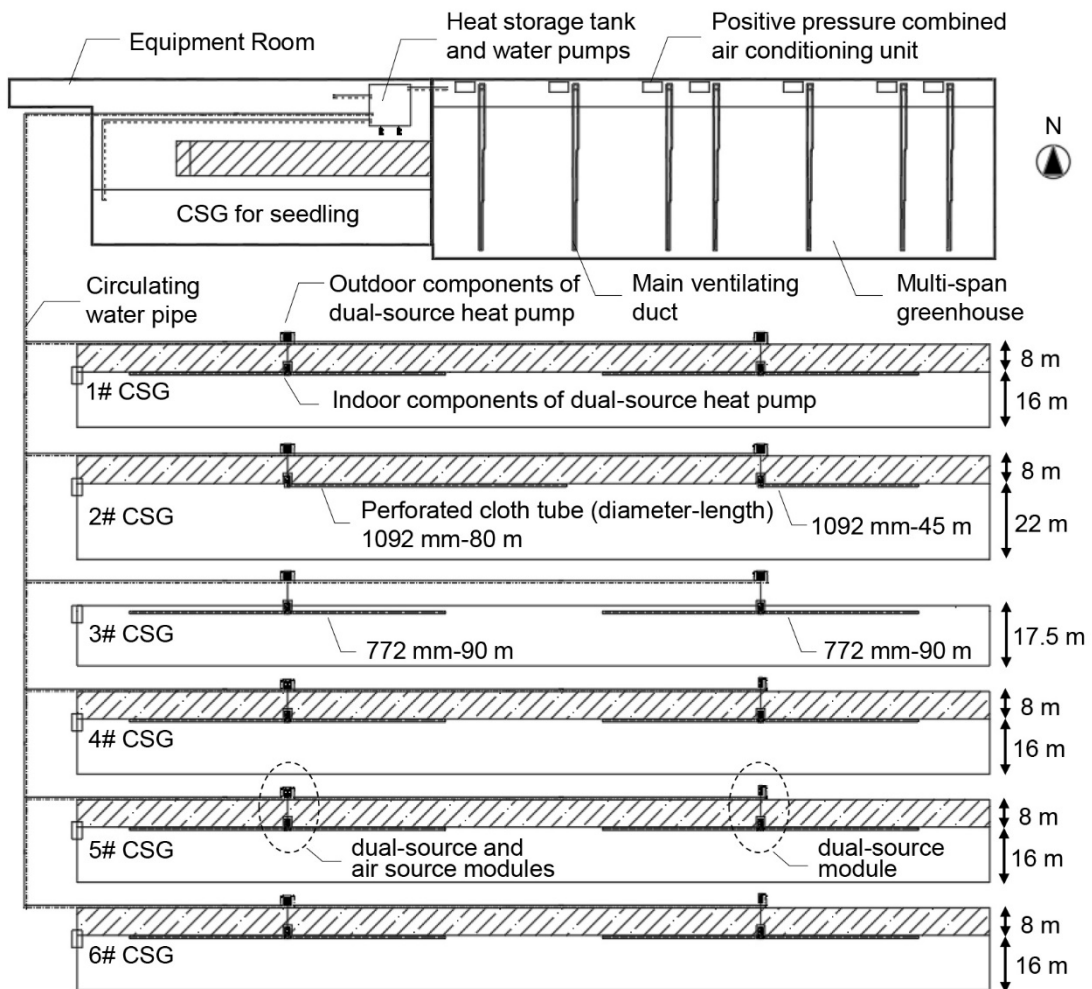


Fig. 7 Layout of the greenhouses and the greenhouse heating system utilizing energy transfer between greenhouses based on a dual source heat pump

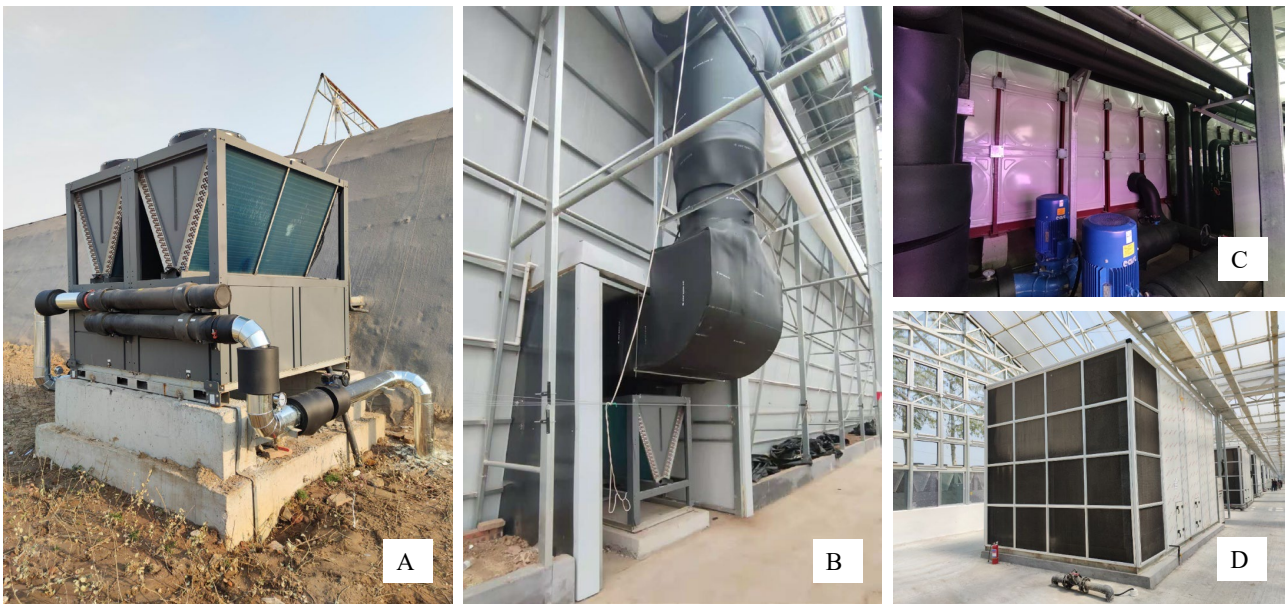


Fig. 8 Pictures of the main components of the greenhouse heating system utilizing energy transfer between greenhouses based on a dual air source heat pump. A: Outdoor components of the dual source heat pump; B: Indoor components of the dual source heat pump and ventilation ducts; C: Heat storage tank and water pumps; D: Combined air conditioning unit.

#### 4.1.1. Heating load of the multi-span greenhouse

Besides the parameterized constants in the heating load model of multi-span greenhouses in Section 3.1, other required parameters for the heating load calculation can be given, following the greenhouse descriptions (Section A1) and local meteorological data. These inputs, and some auxiliary variables, are detailed in Table 2. The energy-saving fraction and switch states of the indoor thermal screen, which was not equipped, are not listed. Simulated results showed that heating loads were different under the three groups of design temperatures. Thus, the maximum value of  $98.2 \text{ W m}^{-2}$  was selected to be the heating load of the multi-span greenhouse.

This case study found that the heating load of the multi-span greenhouse was obtained at the 100% guaranteed rate of indoor air temperature  $\geq t_{g,3}$ . Assuming that this greenhouse is not equipped with an external thermal blanket (i.e., the roof is only covered with a single glass), the heating load will be estimated to be  $293.9 \text{ W m}^{-2}$ , which is also obtained under the same group of design temperatures. Using

traditional methods [48, 61] the design outdoor air temperature takes the average of annual minimum temperatures over the past 20 years in Shouguang (-8.1°C [33]) and the design indoor air temperature takes 16°C, heating loads of the multi-span greenhouse with and without external thermal blanket are 83.5 and 251.5 W m<sup>-2</sup>, respectively. Both are lower than those calculated by the hierarchical valuing method, which means that on extremely low-temperature days, the indoor air temperature will drop to an unacceptable value (below  $t_{g,3}$ ), and the decline will be even more significant for greenhouses heated by air source heat pumps. One may conclude that the heating load model of this study is more transparent and reliable for equipment selection.

The heating load model of multi-span greenhouses is user-friendly for greenhouses with indoor thermal screens and applies to those with external thermal blankets. It also distinguishes greenhouses that cultivate fruiting vegetables and leafy vegetables. With this model, for a 50,000 m<sup>2</sup> Venlo-type glass greenhouse, used for planting fruiting vegetables (with a span of 9.6 m, an eaves height of 6 m, a roof inclination angle of 23°, a roof covered by 5 mm single glass, and a foundation wall height of 0.5 m), the heat transfer coefficient of the greenhouse roof is calculated to be 7.18 W m<sup>-2</sup> °C<sup>-1</sup>, assuming that indoor and outdoor air temperatures are respectively 18 and -12 °C, outdoor wind speed is 4 m s<sup>-1</sup>, and thermal conductivity of glass is 0.8 W m<sup>-1</sup> °C<sup>-1</sup>. The coefficient is higher than the recommended values in some standards without considering radiative processes comprehensively [60, 61]. Meanwhile, the simulated heat transfer coefficients of single glass are closer to measured values rather than those coefficients recommended by standards (Table 3). When the greenhouse is covered by a single PE film (0.1 mm, with thermal conductivity of 0.34 W m<sup>-1</sup> °C<sup>-1</sup>), and view factors for a leafy vegetable greenhouse are adopted, the heat transfer coefficient of the roof is determined to be 10.05 W m<sup>-2</sup> °C<sup>-1</sup>. Since the radiation heat exchange between the indoor radiating body and sky is integrated, simulated coefficients of the single PE film are higher than the recommended and measured values shown in Table 3 but not higher than the measured value in reference [64]. Generally, the heating load model has a good performance.

Table 2 Input parameters and auxiliary variables for heating load calculation of the multi-span greenhouse

Parameters	Value
<b>Greenhouse dimensions</b>	
○ Greenhouse average height $H$ (m)	8.20
○ Greenhouse floor area $A_f$ (m <sup>2</sup> )	8486.4
○ Perimeter of greenhouse $pe$ (m)	430.4
○ Height of sidewalls excluding foundation walls $H_g$ (m).	5.25
● Total surface area of indoor radiating bodies $A_g$ (m <sup>2</sup> )	10746

---

**Design parameters of indoor and outdoor climate**

○ Design indoor air temperature $t_g$ (°C)	18	14	10
○ Design outdoor air temperature $t_a$ (°C)	-5.5	-7.4	-18.7
○ Outdoor wind speed $v$ (m s <sup>-1</sup> )		4	
● Effective sky temperature $t_{sky}$ (°C)	-31.4	-34.0	-49.1

---

**Roof**

○ Surface area $A_c$ (m <sup>2</sup> )		8137	
● Convective coefficient of the internal surface $h_{c,in}$ (W m <sup>-2</sup> °C <sup>-1</sup> )	3.09	3.04	3.30
● Convective coefficient of the external surface $h_{c,out}$ (W m <sup>-2</sup> °C <sup>-1</sup> )		22.56	
○ Thermal conductivity of external thermal blanket (35 mm) $\lambda_{c,i}$ (W m <sup>-1</sup> °C <sup>-1</sup> )		0.06 <sup>a</sup>	
○ Thermal conductivity of single glass (5 mm) $\lambda_{c,i}$ (W m <sup>-1</sup> °C <sup>-1</sup> )		0.8	
○ Emissivity of the external surface $\varepsilon_{c,out}$ (-)		0.75	
○ Transmittance to long-wave radiation $\tau_c$ (-)		0	
● Apparent radiation heat transfer coefficient between the internal surface and indoor radiating body $r_{c,in}^*$ (W m <sup>-2</sup> °C <sup>-1</sup> )	4.27	4.10	3.91
● Apparent radiation heat transfer coefficient between the external surface and sky $r_{c,out}^*$ (W m <sup>-2</sup> °C <sup>-1</sup> )	-45.58	-42.12	-57.15
● Apparent radiation heat transfer coefficient between indoor radiating body and sky $r_{c,t}^*$ (W m <sup>-2</sup> °C <sup>-1</sup> )	0	0	0
● View factor of indoor radiating body to the internal surface $F_{g,c}$ (-)		0.70	
● Internal surface temperature $t_{c,in}$ (°C)	13.3	9.6	4.3
● External surface temperature $t_{c,out}$ (°C)	-7.0	-9.0	-19.9
● Overall heat transfer coefficient $U_c$ (W m <sup>-2</sup> °C <sup>-1</sup> )	1.47	1.47	1.43

---

**Gutter**

○ Surface area $A_c$ (m <sup>2</sup> )		998.4	
● Convective coefficient of the internal surface $h_{c,in}$ (W m <sup>-2</sup> °C <sup>-1</sup> )	2.50	2.45	2.68
● Convective coefficient of the external surface $h_{c,out}$ (W m <sup>-2</sup> °C <sup>-1</sup> )		22.96	
○ Thermal conductivity of polystyrene board (50 mm) $\lambda_{c,i}$ (W m <sup>-1</sup> °C <sup>-1</sup> )		0.04 <sup>b</sup>	
○ Emissivity of the external surface $\varepsilon_{c,out}$ (-)		0.4	
○ Emissivity of the internal surface $\varepsilon_{c,in}$ (-)		0.85	
○ Transmittance to long-wave radiation $\tau_c$ (-)		0	
● Apparent radiation heat transfer coefficient between the internal surface and indoor radiating body $r_{c,in}^*$ (W m <sup>-2</sup> °C <sup>-1</sup> )	4.70	4.51	4.31
● Apparent radiation heat transfer coefficient between the external surface and sky $r_{c,out}^*$ (W m <sup>-2</sup> °C <sup>-1</sup> )	-42.46	-39.53	-52.73
● Apparent radiation heat transfer coefficient between indoor radiating body and sky $r_{c,t}^*$ (W m <sup>-2</sup> °C <sup>-1</sup> )	0	0	0
● View factor of indoor radiating body to the internal surface $F_{g,c}$ (-)		0.09	
● Internal surface temperature $t_{c,in}$ (°C)	15.6	11.7	7.0
● External surface temperature $t_{c,out}$ (°C)	-6.4	-8.3	-19.4

● Overall heat transfer coefficient $U_c$ ( $\text{W m}^{-2} \text{ }^\circ\text{C}^{-1}$ )	0.75	0.75	0.74
<b>Side wall</b>			
○ Surface area above foundation wall $A_c$ ( $\text{m}^2$ )		2619.6	
● Convective coefficient of the internal surface $h_{c,in}$ ( $\text{W m}^{-2} \text{ }^\circ\text{C}^{-1}$ )	3.20	3.14	3.41
● Convective coefficient of the external surface $h_{c,out}$ ( $\text{W m}^{-2} \text{ }^\circ\text{C}^{-1}$ )		22.56	
○ Thermal conductivity of three-glass and two-cavity tempered insulating glass (27 mm) $\lambda_{c,i}$ ( $\text{W m}^{-1} \text{ }^\circ\text{C}^{-1}$ )		0.05 <sup>a</sup>	
○ Transmittance to long-wave radiation $\tau_c$ (-)		0	
● Apparent radiation heat transfer coefficient between the internal surface and indoor radiating body $r_{c,in}^*$ ( $\text{W m}^{-2} \text{ }^\circ\text{C}^{-1}$ )	4.00	3.84	3.65
● Apparent radiation heat transfer coefficient between the external surface and sky $r_{c,out}^*$ ( $\text{W m}^{-2} \text{ }^\circ\text{C}^{-1}$ )	-43.88	-40.80	-53.71
● Apparent radiation heat transfer coefficient between indoor radiating body and sky $r_{c,t}^*$ ( $\text{W m}^{-2} \text{ }^\circ\text{C}^{-1}$ )	0	0	0
● View factor of indoor radiating body to the internal surface $F_{g,c}$ (-)		0.21	
● Internal surface temperature $t_{c,in}$ ( $^\circ\text{C}$ )	12.8	9.1	3.7
● External surface temperature $t_{c,out}$ ( $^\circ\text{C}$ )	-7.2	-9.3	-20.1
● Overall heat transfer coefficient $U_c$ ( $\text{W m}^{-2} \text{ }^\circ\text{C}^{-1}$ )	1.58	1.59	1.54
<b>Heating load</b>			
● Combined heat transfer through cover $Q_{tr}$ ( $\text{W m}^{-2}$ )	46.54	42.59	55.42
● Infiltration heat loss $Q_v$ ( $\text{W m}^{-2}$ )	35.00	31.87	42.75
● Greenhouse heating load $Q_h$ ( $\text{W m}^{-2}$ )	81.54	74.46	98.17

Note: a denotes the average thermal conductivity coefficient of the composite layer, which is the effective property. b indicates that the influence of steel plate at the external layer on gutter thermal resistance is ignored. ○ denotes input parameters; ● denotes auxiliary variables.

Table 3 Comparison of measured, simulated, and standard heat transfer coefficients of typical cover materials for multi-span greenhouses

Cover material	Outdoor air temperature ( $^\circ\text{C}$ )	Indoor air temperature ( $^\circ\text{C}$ )	Outdoor wind speed ( $\text{m s}^{-1}$ )	Heat transfer coefficients		
				Measured ( $\text{W m}^{-2} \text{ }^\circ\text{C}^{-1}$ ) [77]	Simulated ( $\text{W m}^{-2} \text{ }^\circ\text{C}^{-1}$ )	Standard ( $\text{W m}^{-2} \text{ }^\circ\text{C}^{-1}$ ) [56, 60, 61]
Single glass	-1.3	27.5	1.0	6.60	6.64	6.2-6.4
Single glass	-2.3	28.3	3.0	7.59	7.23	6.2-6.4
Single glass	-2.3	27.8	5.0	8.61	7.60	6.2-6.4
Single PE film	-1.3	27.8	1.0	8.11	9.57	6.2-6.8
Single PE film	-2.5	27.0	2.1	8.67	10.01	6.2-6.8
Single PE film	-2.0	26.3	3.0	8.81	10.32	6.2-6.8

#### 4.1.2. Surplus air heat inside CSGs

The dimensions and materials of the heat source CSGs are detailed in Section A2. According to the surplus air heat model of CSGs proposed in Section 3.2, the required input parameters, and some in-process results, are detailed in Table 4. The calculated results showed that the available surplus air heat in closed CSGs ranged from 154.7 to 177.4 W m<sup>-2</sup>, while it had a range of 100.8-112.6 W m<sup>-2</sup> considering the roof ventilation, which was more suitable for system sizing. Thus, the sum of surplus air heat from the six CSGs for equipment selection was 3004.5 kW.

The developed surplus air heat model of CSGs considers the main long-wave radiative processes, improving simulation accuracy while ensuring simplicity. It explains the influences of shading on solar radiation received by the north roof, north wall, and indoor floor and avoids too-large simulated values at high solar altitude [47, 78]. Meanwhile, the model is compatible with closed and ventilated CSGs to cope with different managements of heat source greenhouses. If we uniformly use the reference indoor air temperature to evaluate excess heat generation, surplus air heat should be equivalent to excess heat inside CSGs. Adding different heat collection devices will change the surplus air heat to varying degrees. It is not easy to measure the accurate surplus air heat inside CSGs. In previous tests, the CSG excess heat could be harvested at a maximum daily average rate of 42-53 W m<sup>-2</sup> [36, 37], indicating that the simulations are satisfactory in guiding the design of CSG energy utilization systems, at least from a qualitative point of view.

Table 4 Input parameters and in-process results for simulating the CSG surplus air heat

Parameters	Value		
	1# & 4-6#	2#	3#
<b>Greenhouse profile</b>			
CSG ridge height $H_{rid}$ (m)	7	8	7
Mean height of the CSG based on indoor floor $H_C$ (m)	5.25	6	4.8
CSG span $L_{fC}$ (m)	16	22	17.5
Floor area $A_{fC}$ (m <sup>2</sup> )	4240	5830	4637.5
Connecting line between roof ridge and bottom angle of north wall $L_{cl1}$ (m)	7.1	8.1	7.5
Connecting line between bottom angle of south roof and apex of north wall $L_{cl2}$ (m)	19	25	17.6
Angle between $L_{cl1}$ and north wall $\theta_{cl1}$ (°)	10	8	9
Infiltration rate of the CSG $N_C$ (h <sup>-1</sup> )		0.4	
<b>North wall</b>			

Height $L_{nw}$ (m)	6	7	7
Surface area $A_{nw}$ (m <sup>2</sup> )	1676.9	1929.2	1908
Angle with indoor floor $\theta_{nw}$ (°)	108	106	78
Absorption ratio of the internal surface to solar radiation $\alpha_{nw,in}$ (-)		0.75	
Thermal conductivity of soil wall (average 5000 mm) $\lambda_{nw,i}$ (W m <sup>-1</sup> °C <sup>-1</sup> )	0.83	0.83	-
Thermal conductivity of polystyrene board (200 mm) $\lambda_{nw,i}$ (W m <sup>-1</sup> °C <sup>-1</sup> )	-	-	0.04
Thermal conductivity of cement mortar at the internal surface (20 mm) $\lambda_{nw,i}$ (W m <sup>-1</sup> °C <sup>-1</sup> )	0.93	0.93	-
Thermal conductivity of cement mortar at the external surface (20 mm) $\lambda_{nw,i}$ (W m <sup>-1</sup> °C <sup>-1</sup> )	0.93	0.93	0.93
Emissivity of the internal surface $\varepsilon_{nw,in}$ (-)	0.94	0.94	0.85
<b>North roof</b>			
Height $L_{nr}$ (m)	1.5	1.5	1.1
Surface area $A_{nr}$ (m <sup>2</sup> )	397.5	397.5	291.5
Angle with the indoor floor $\theta_{nr}$ (°)	34	34	0
Absorption ratio of the internal surface to solar radiation $\alpha_{nr,in}$ (-)		0.75	
Thermal conductivity of cement mortar at the external surface (20 mm) $\lambda_{nr,i}$ (W m <sup>-1</sup> °C <sup>-1</sup> )	0.90	0.90	0.90
Thermal conductivity of soil layer (average 2000 mm) $\lambda_{nr,i}$ (W m <sup>-1</sup> °C <sup>-1</sup> )	0.83	0.83	-
Thermal conductivity of non-woven fabric (3.5 mm) $\lambda_{nr,i}$ (W m <sup>-1</sup> °C <sup>-1</sup> )	0.06	0.06	-
Thermal conductivity of polystyrene board (45 mm) $\lambda_{nr,i}$ (W m <sup>-1</sup> °C <sup>-1</sup> )	-	-	0.04
Emissivity of the internal surface $\varepsilon_{nr,in}$ (-)	0.05	0.05	0.85
<b>Indoor floor and soil</b>			
Absorption ratio of indoor floor to solar radiation $\alpha_{fC}$ (-)		0.92	
Thermal conductivity of soil $\lambda_s$ (W m <sup>-1</sup> °C <sup>-1</sup> )		0.83	
Soil depth of constant temperature $\delta_{cs}$ (m)		3	
Constant soil temperature $t_{cs}$ (°C)		15	
Emissivity of indoor floor $\varepsilon_{fC}$ (-)		0.96	
<b>South roof</b>			
Arc length $L_{sr}$ (m)	19	25.1	17
Surface area $A_{sr}$ (m <sup>2</sup> )	5035	6651.5	4823
Angle with indoor floor $\theta_{sr}$ (°)	22	19	25
Total transmittance to solar radiation $\zeta$ (-)		0.78	
Thermal conductivity of polyolefin film (0.15 mm) $\lambda_{sr,i}$ (W m <sup>-1</sup> °C <sup>-1</sup> )		0.13	
Emissivity of the internal surface $\varepsilon_{sr,in}$ (-)		0.15	
Emissivity of the external surface $\varepsilon_{sr,in}$ (-)		0.15	
Transmittance for long wave radiation $\tau_{sr}$ (-)		0.75	
<b>Design climate parameters</b>			
Design indoor air temperature $t_{gC}$ (°C)		28	
Design outdoor air temperature $t_a$ (°C)		13.5	

Indoor wind speed $v_{gC}$ (m s <sup>-1</sup> )			1
Outdoor wind speed $v$ (m s <sup>-1</sup> )			0.5
Outdoor solar radiation in horizontal direction $I_{f,out}$ (W m <sup>-2</sup> )			480.6
Solar altitude $\theta_{sun}$ (°)			36
<b>Temperatures of envelop surfaces</b>			
Internal surface temperature of north wall $t_{nw,in}$ (°C)	56.4	55.8	47.7
Internal surface temperature of north roof $t_{nr,in}$ (°C)	26.1	26.1	23.0
Indoor floor temperature $t_{fC}$ (°C)	41.1	40.9	42.0
Internal surface temperature of south roof $t_{sr,in}$ (°C)	21.5	21.5	21.4
External surface temperature of south roof $t_{sr,out}$ (°C)	21.4	21.4	21.3
<b>Surplus air heat of the CSG <math>Q_s</math> (W m<sup>-2</sup>)</b>			
When greenhouse is closed	177.4	154.7	160.0
When roof windows are opened (open width $L_v = 0.15$ m)	112.6	107.6	100.8

### 4.1.3. Sizing Heat pumps

The heating load of the CSG for seedling production (1600 m<sup>2</sup>) took a value of 60 W m<sup>-2</sup>. The equipment room that needed heating had an area of 2460 m<sup>2</sup>. Its heating load value took 25 W m<sup>-2</sup>, mainly for freeze protection. Therefore, the sum of the heating load for the multi-span greenhouse, the CSG for seedling production, and the equipment room was 992.9 kW. Since the multi-span greenhouse was the main source of heating load, for simplification, we focused on the multi-span greenhouse condition for the following equipment selection instead of comparing heating schemes among the three sites.

According to fitting functions in Fig. 6, when the ambient air temperature was -18.7 °C, and the outlet water temperature was 45 °C, the COP and input power of the selected heat pump module (Section A3) were 2.2 and 21.4 kW, respectively. In line with Eqs. (45), as the extra coefficient  $\beta_{hp}$  took 1, the rated heating capacity of the air source heat pump  $HP_{a,rc}$  was calculated to be 1799.6 kW. Therefore, 20.9 (rounded to 21) heat pump modules needed configuration, and the installed capacity  $HP_{a,ins}$  was determined to be 1803.9 kW. Then, in line with Eqs. (46), the rated capacity of heat pump modules that adopted double heat sources  $HP_{d,rc} = HP_{a,ins} = 1803.9$  kW. All the 21 heat pump modules should be dual source since the accumulated surplus air heat from the six CSGs was excessive, while the total heating demand in a heating cycle was large enough. And according to Eqs. (49), the available surplus air heat of CSGs should not be less than 1778.5 kW, which could be satisfied since the six CSGs had a gross surplus air heat of 3004.5 kW.

Based on the above calculations for equipment selection, 21 air source heat pump modules were built in

this case study, from which only 12 modules were extended to have double sources due to the investment limitation. As a result, the actual installed capacity of the dual source heat pump  $HP_{d,ins}$  was 1030.8 kW. These dual source modules were evenly distributed to the six CSGs. Accordingly, the ETGHP system was designed with 12 sets of heat pump units that each included one dual source module and either a zero or one single-source module (Fig. 7). However, this compromise provided an opportunity to compare the performance of heat pumps with different heat sources because the CSG air source and outdoor air source heating conditions could co-occur.

#### 4.1.4. Sizing heat storage tank

According to Eqs. (47), the effective volumes of the heat storage tank under  $HP_{d,rc}$  and  $HP_{d,ins}$  conditions were determined to be 435.5 and 248.9 m<sup>3</sup>, respectively. The installed water tank was assembled by glass fiber reinforced polymer plates. It had an effective volume of approximately 500 m<sup>3</sup>, meeting the requirements. The tank storing heat, collected by the heat pump during the day, also acts as a short-term buffer. For example, the heat pump can be turned on in advance instead of waiting for the temperature threshold of inlet water on cold nights, making up for the shortage of the heat pump capacity. In other words, the buffer tank can help reduce the installed capacity of the air source heat pump by avoiding peak loads.

#### 4.1.5. Sizing fan and surface air cooler

According to the summer demands for ventilation and cooling, seven combined air conditioning units were designed and installed in the multi-span greenhouse. Each unit had a supply power of 380V, a rated input power of 30 kW, a rated airflow of 65000 m<sup>3</sup> h<sup>-1</sup>, and a residual pressure of 750 Pa. Each unit was equipped with a frequency changer. The units were installed in the equipment room (Fig. 7), with external windows connecting to the outdoors and internal windows relating to the greenhouse cultivation space. In the heating process, external windows were closed, and internal windows were opened, generating an internal air circulation pattern. The rated capacity of each surface air cooler was determined to be 166.0 kW based on Eqs. (48), and the actual installed capacity of 225 kW could meet this demand. This configuration allowed the fan to run below 40 Hz for warm air distribution.

#### 4.1.6. Area Matching between CSGs and the multi-span Greenhouse

For the area matching study, the heating load of the multi-span greenhouse was considered. Taking the

specifications of CSG 1# and CSG 3# as examples, the areas of CSGs should not be less than 15795 and 17644 m<sup>2</sup>, respectively, according to Eqs. (49). Therefore, to use the ETGHP system to heat a multi-span greenhouse with an external thermal blanket, the minimum area of CSGs required as heat sources was roughly twice the multi-span greenhouse area. However, it is essential to note that, in this case study, the matching ratio was determined by the installed capacity of the air source heat pump rather than the greenhouse heating load. If we only considered the relationship of energy supply and demand between greenhouses, this critical matching ratio would be 2.3-2.5, which might apply to other heating systems utilizing energy transfer between greenhouses.

## 4.2. System application

Two consecutive days from 9:00 on January 17 to 9:00 on January 19, 2021 (i.e., two heating cycles) were selected to introduce running states of the ETGHP system. Based on the data, the application effect and performance of the system were preliminarily evaluated. The weather conditions of the two days were sunny (Fig. 4). The cumulative outdoor solar radiation was 10.69 and 11.05 MJ m<sup>-2</sup> d<sup>-1</sup>, with the maximum radiation of 533.8 and 565.0 W m<sup>-2</sup>, respectively. The multi-span greenhouse was producing tomatoes. A sub-optimal setting of indoor air temperature was performed since the thermal insulations were not enabled during the test. Fruiting vegetables were cultivated in the six heat source CSGs and managed independently by different growers.

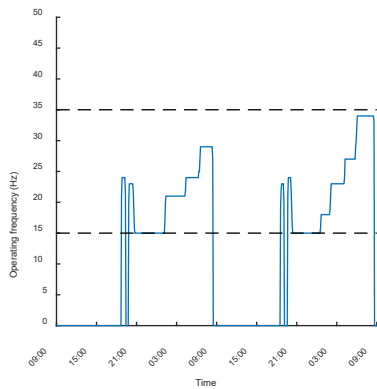
Outdoor climate data were measured by the HOBO U30 weather station (Onset Computer Corporation, USA). Indoor climate, water temperature, and compressor current were monitored and recorded by the system-provided sensors and platforms. The water flow was measured by a KRC-1518H ultrasonic flowmeter (Kecrichen (Dalian) Instrument Development Co., Ltd., China) with a volume flow accuracy of ±1%.

### 4.2.1 Running status

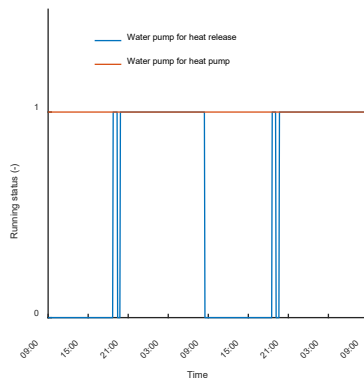
Following the system control scheme described in Section A4, the specific operation settings over the two heating cycles are shown in Table 5. The ETGHP system operated according to such settings, and its actual running states can be seen in Fig. 9.

Table 5 Operation settings of the ETGHP system

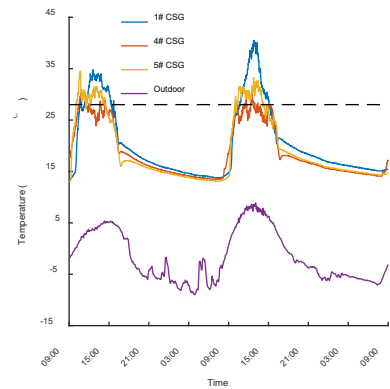
Operating parameters		Setpoints
$t_{g,low}$ (°C)		12
$t_{g,up}$ (°C)		14
$t_{inl,up}$ (°C)	In the day	45
	At night	30
$\Delta t_{inl}$ (°C)		5
$t_{gC,up}$ (°C)		28
$\Delta t_{gC}$ (°C)		2
$\phi_{low}$ (Hz)		15
$\phi_{up}$ (Hz)		35
Circulating water flows for heat pumps $v_{hp}$ (m <sup>3</sup> h <sup>-1</sup> )	Module 01 of unit 1#E	16.5
	Module 02 of unit 1#E	14.3
	Module 01 of unit 4#W	15.2
	Module 02 of unit 4#W	15.2
	Module 01 of unit 5#E	21.2



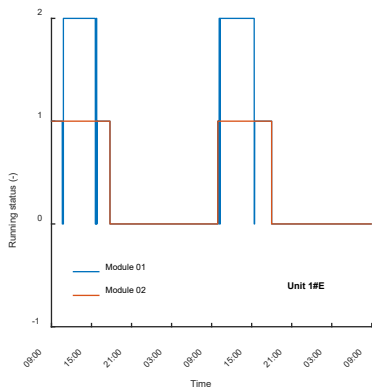
(a)



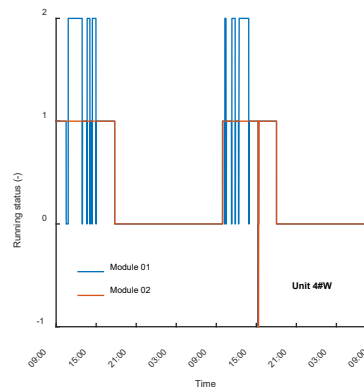
(b)



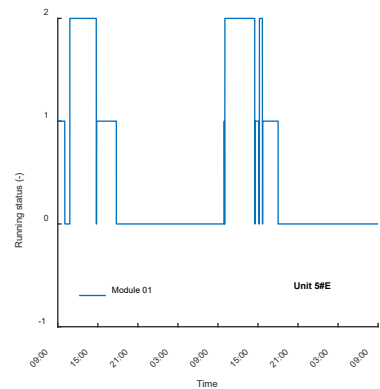
(c)



(d)



(e)



(f)

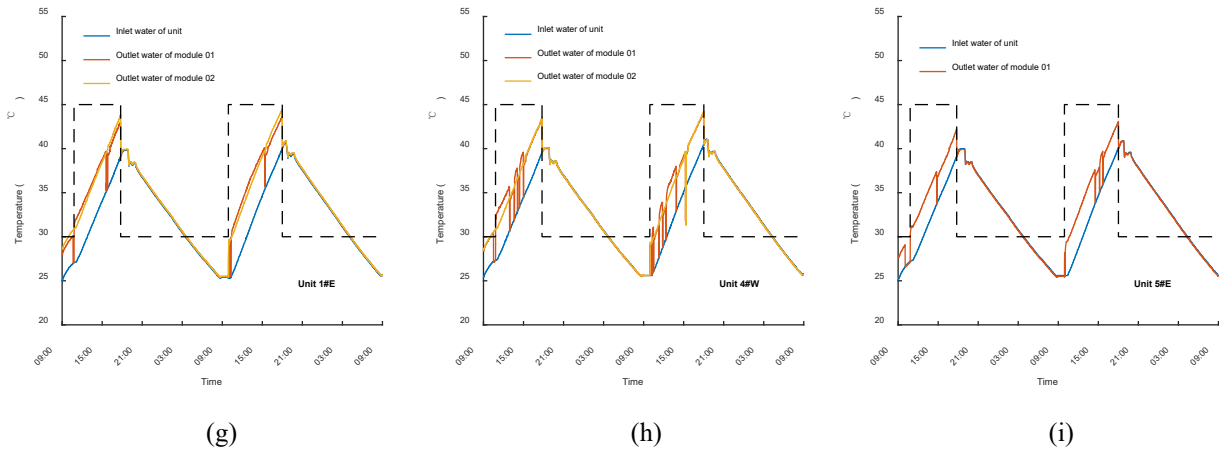


Fig.9 Running states of the ETGHP system and its components. Data are selected from Jan. 17 to Jan. 19, 2021. (a) Output frequency of fans. (b) Running status of water pumps. 0 denotes off, and 1 denotes on. (c) Temperatures of heat sources. CSG denotes the Chinese solar greenhouse. (d) Running status of compressors of 1#E heat pump unit. Module 01 of the heat pump unit has double heat sources, and module 02 has a single heat source. For the compressor running status, 0 denotes off, 1 denotes on at the outdoor air source heating mode, 2 denotes on at the CSG air source heating mode, and -1 denotes on at the defrosting mode. The same is below. (e) Running status of compressors of 4#W heat pump unit. (f) Running status of compressors of 5#E heat pump unit. (g) Water temperatures of 1#E heat pump unit. (h) Water temperatures of 4#W heat pump unit. (i) Water temperatures of 5#E heat pump unit.

As shown in Fig. 9a, the average running time of the fans was 13.29 h per day. During the initial heating period at night, the multi-span greenhouse air temperature could easily exceed the upper bound, resulting in intermittent starts and stops of fans due to the high temperature of water flowing through surface air coolers. After that, the fans ran stably but with increasing output frequency due to the decreased inlet water temperature and the heating requirement variation. The average daily running time of the water pump for heat release was 13.29 h, and 24 h for heat pump heating(Fig. 9b).

Running states of the representative heat pump units and modules are illustrated in Fig. 9c-9i. For instance, the running states of module 01 of unit 1#E in one heating cycle (Jan. 18 to Jan. 19, 2021) are as follows:

- From 9:00 to 9:54, there was no heating requirement in the multi-span greenhouse, and the fan was not running. The inlet water temperature of the heat pump unit was constant at 25.4 °C, which did not drop to the lower limit ( $t_{inl,up}-\Delta t_{inl}$ ) of 25°C at this stage. Thus, the heat pump was not running.

- From 9:55, the inlet water temperature setpoint for stopping the heat pump  $t_{inl,up}$  was adjusted to 45 °C. So, the inlet temperature was lower than  $t_{inl,up} - \Delta t_{inl}$  (40 °C). Meanwhile, the air temperature inside the CSG was 25.8 °C, which was lower than the reference temperature for generating surplus air heat  $t_{gC,up}$  (28 °C). The heat pump ran under the outdoor air source heating condition. This period lasted for 0.16 h, during which the average temperature difference between inlet and outlet water of the heat pump module was 3.4 °C.
- At 10:05, the CSG air temperature rose to 28.0 °C. The heat pump stopped and got ready to switch to the CSG air source heating mode. This downtime was 0.05 h.
- Then, at 10:08, the CSG air temperature was 28.6 °C and higher than  $t_{gC,up}$ . The heat pump started to run under the CSG condition. Due to the heat extraction, the CSG air temperature dropped rapidly to 26.0 °C at 10:14, triggering the stop of the heat pump and preparing to switch to the outdoor mode. This stage lasted only 0.12 h, and the average water temperature difference was 4.1 °C.
- However, after the setup time, the CSG air temperature rose back to 28.7 °C at 10:18. The heat pump still started to run with the CSG condition until 15:22. This stage lasted for 5.08 h, during which the CSG air temperature was 26.2-40.5°C, and the average water temperature difference was 5.2 °C.
- At 15:23, the CSG air temperature dropped to 25.9 °C. The heat pump stopped for 0.05 h and prepared to switch to the outdoor mode.
- From 15:27 to 17:59, the heat pump ran continuously with the outdoor condition, during which the temperature difference was 3.8 °C. At the end of this stage, the inlet water temperature of the heat pump reached 40 °C.
- At 18:00,  $t_{inl,up}$  was adjusted to 30 °C, and the heat pump stopped running. Until 9:00 on Jan. 19, the inlet water temperature was always higher than 25 °C, and the heat pump did not run.

Module 02 of unit 1#E had the same initial start and final stop times as module 01. It ran 8.06 h continuously without switching heat sources. The control rules of other heat pump units were similar to unit 1#E. However, due to the differences in greenhouse management and heat pump setpoints, sensor measurement errors, and equipment operation faults, these units differed in specific running conditions. For instance, in the selected two heating cycles, the running time of unit 1#E under the CSG air source heating condition (10.01 h) was longer than that of unit 5#E (8.86 h) and much longer than that of unit 4#W (5.10 h). Furthermore, unit 4#W switched heat sources more often following the CSG air temperature variation. During the running of the heat pump under the outdoor air source heating condition, the defrosting condition was timely started according to the evaporator frosting situation. The inlet water temperature of the heat pump unit could estimate the water temperature of the heat storage tank, which would be slightly undervalued.

The use efficiency of excess CSG energy has not been revealed without a surplus air heat model. Instead, the heat storage medium temperature could be an indicator to assess the potential of system heating and CSG energy utilization. In this case study, the water tank temperature was set to an upper limit of 45°C (Table 5). It reached 35.4°C by heat pump using CSG air source and exceeded 40°C by an extra run of the heat pump in outdoor mode (Fig. 9d & 9g). The attainable maximum water tank temperature is higher than that achieved by the active solar heat storage-release systems [37, 38] and water-flowing roof skeleton network [41], which had a range of 20-26°C. Some other water cycling systems, with improved collector and optimized heat storage volume, can also raise the water temperature to around 35°C [34-36]. However, they cannot eliminate the heat collection efficiency decrease with the increase of water temperature caused by convections with indoor air. It is tricky to improve these systems to break through temperature limits in heat storage since their heat collectors should always balance the heat release capacity. As a result, a situation will quickly occur where the existing CSG energy utilization systems no longer collect heat effectively or even emit heat, even if there is a great deal of excess energy. This situation worsens in practice, considering the growers must open vents for air exchange and to control air temperature not exceeding 32°C for crop needs. The ETGHP system, which collects heat by compressor-driven heat pump cycle, enabling heat storage medium separate from indoor air, can overcome the convection restriction and obtain 45°C or even higher temperature [13, 55]. Thus, compared with previous studies, the ETGHP system offers more potential for CSG excess energy utilization in heat collection while requiring more driven electric energy.

As expected in northern China for commercial production, the daily average time of greenhouse heating exceeded 13 h (Fig. 9a & 9b). Inputting heat energy to the multi-span greenhouse during this time is compulsory due to the enormous heating requirement presented in Section 4.1.1. In comparison, the heat release time of the existing CSG energy utilization systems was reported to be 3.7-8.5 h on a daily average, and only 53-80% of the collected heat was released, mainly because there was not enough energy sink to consume such heat efficiently and timely [34, 37]. On most nights, the collected energy stagnated, thus, leading to a decrease in heat collection in the daytime [35]. Although free energy, it deserves a more sustainable solution. The ETGHP system, modifying the self-sufficient mode to energy integration, can undoubtedly achieve higher use efficiency of collected heat; thus, CSG surplus air heat. For instance, on each of the selected two days, the heat collected from CSGs during the day was used entirely at night (Fig. 9g-9i). In short, the above discussions based on running states indicate that this study can improve the CSG energy use efficiency from both heat collection and release perspectives.

#### 4.2.2. Heating effect

According to the setpoints (Table 5), the air temperature inside the multi-span greenhouse heated by the ETGHP system was maintained within a range of 11.8-14.0 °C during the heating period, with the average temperature being 12.7 °C (Fig. 10). The temperature difference between indoor and outdoor air was 18.1 °C on average and peaked at 21.3 °C. Taking CSG 1#, 4#, and 5# as examples, the average air temperature inside CSGs was 14.8-17.0°C at night (17:00-07:00 the next day), with the lowest temperature being 13.1°C (Fig. 9c). While running the heat pump, taking CSG surplus air heat as the heat source, the CSG air temperature was not lower than 26 °C and remained high. The ETGHP system had a stable heating effect for the multi-span greenhouse, while its application did not make against the thermal performances of CSGs.

The dual source system design contributes to the heating stability since the CSG surplus air heat roots in the unstable solar radiation. In essence, the system adopts an air/air dual source heat pump that switches parallelly arranged CSG and outdoor air sources, prioritizing air inside CSGs. Then as the available surplus air heat was insufficient, the outdoor air source aided it (Fig. 9). This heat pump presents a more straightforward arrangement and control compared to the existing solar/air [51, 52] and ground/air [53, 54] methods. As the external thermal blanket is enabled for the multi-span greenhouse, a more competitive heating effect will be obtained.

The ETGHP system only extracts the heat that should have been discharged, which will not adversely affect crop growth and the nighttime thermal performance of CSGs. However, considering capital costs, a well-designed system cannot always remove all the excess heat. For example, the maximum air temperature inside CSG 1# still exceeded 40°C during heat collection (Fig. 9c & 9d), causing high-temperature stress to crops. As discussed, ventilation is inevitable, especially during the peak period of excess heat. Hence, a model predictive control of vents is preferred to maintain a temperature range, tolerating crop growth and heat collection. In addition, CSG heating, though necessary in some weather, is not the concern of this article and might be involved in future system design.

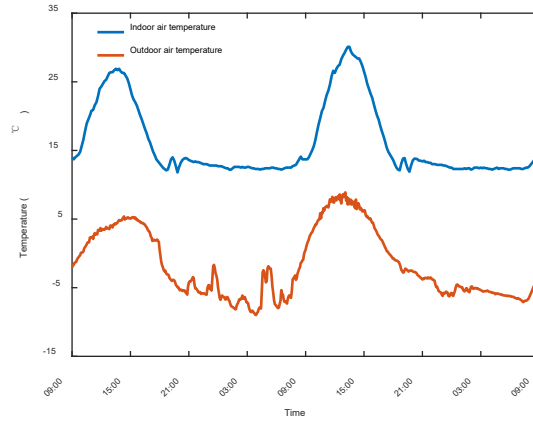


Fig.10 Variation of air temperatures inside and outside the multi-span greenhouse (from Jan.17 to Jan.19, 2021)

#### 4.2.3. Performance of heat pumps

Taking units 1#E, 4#W, and 5#E as examples, the heating performance of the heat pump was analyzed.

COP of the heat pump adopted the following calculations:

$$COP = \frac{HP}{E} \quad (-) \quad (50)$$

$$HP = \frac{1}{3600} v_{hp} \rho_w c_{p,w} (t_{outl} - t_{inl}) \quad (W) \quad (51)$$

Where  $COP$  (-) is the coefficient of heating performance of the heat pump;  $HP$  (W) is the heat output of the heat pump;  $E$  (W) is electric power consumption by heat pump, excluding water pumps; the fan is assumed to run with rated electric power input;  $v_{hp}$  ( $m^3 h^{-1}$ ) is the flow rate of circulating water passing through the heat pump;  $t_{inl}$  and  $t_{outl}$  ( $^{\circ}C$ ) are inlet and outlet water temperatures of the heat pump condenser, respectively.

The input power of the heat pump compressor  $E_{com}$  (W) was calculated by:

$$E_{com} = \sqrt{3} U_{com} I_{com} \cos\varphi \quad (W) \quad (52)$$

Where  $U_{com} = 380$  V is the compressor operating voltage;  $I_{com}$  (A) is the compressor running current;  $\cos\varphi = 0.92$  is the power factor. The running currents of heat pump compressors are presented in Fig. 11.

Circulating water flow rates, as well as inlet and outlet water temperatures of the heat pumps, can be obtained from Table 5 and Fig. 9g-9i, respectively.

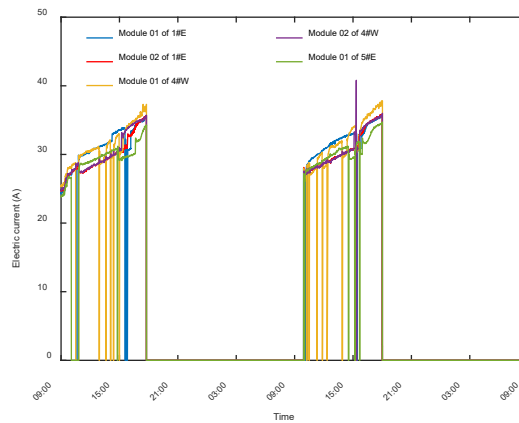


Fig.11 Electric currents of heat pump compressors (from Jan.17 to Jan.19, 2021)

The heating performances of dual source modules and air source modules of the heat pump units are presented in Tables 6 and 7, respectively. In the selected two heating cycles, the COP of the dual source heat pump modules, when using CSG surplus air heat as the heat source, was 4.3-4.8, while the COP of the air source modules was 3.4-3.7, over the same period. The COP was improved by 23-26% due to using the higher-grade heat source of CSG air rather than ambient air. Throughout the entire heat collection period, the dual source heat pumps switched heat sources between indoor and outdoor air according to their setting and the variation of CSG air temperatures. Their total COP, which considered both CSG and outdoor air source heating conditions, reached 3.4-4.2, a 6-11% increase compared to air source heat pumps.

The heat source above 26°C enabled the dual source heat pump to increase its COPs compared to the air source heat pump. Thus, a conclusion can be reached that the ETGHP system can transfer energy between greenhouses for greenhouse heating by efficiently using the air source heat pump, creating enormous potential for energy savings. The COP of the heat pump under the CSG air source condition is slightly higher than that obtained in the self-sufficient scenario (3.3-4.2 [46]), mainly because the COP of this study did not consider the power consumption of water pumps, and the heat pump manufacturing process was improved. The heat pump in CSG mode also performs better than the heat pump indirectly using surplus air, with a water source of approximately 15°C and daily mean COP of 2.3-3.6 [29], as well as ground source heat pumps, ranging COP in 2.3-3.9 [15-17, 79]. However, it experiences uncertainties in the heat source supply time. Meanwhile, the total COP of the dual source heat pump, as expected by the original design intention [55], has been improved, but to a different level from other similar heat pumps [51, 53, 54].

The heat pump units differed in heating performances. One reason could be that their working conditions were not entirely uniform. Another reason might be ascribed to manufacturing process issues. The dual source heat pump switched heat sources, and the refrigerant might have been entrapped in the off-working evaporator, which led to different flow rates of working fluids that affected the COPs.

This study obtained the COP increases of the heat pump by using CSG air rather than ambient air. However, the outdoor air temperature did not become too low over the two selected days, with an average of 5.2 °C from 10: 00 to 15: 00. As outdoor temperature decreases further, the COP of the air source heat pump also decreases, and the cumulative defrosting time increases [23], while the CSG surplus air heating condition remains the same. In this scenario, the comparative advantage of the heat pump under CSG conditions would increase. In contrast, available excess heat decreases in colder weather, so the running time of the heat pump under CSG conditions would become shorter, resulting in lower total COP. Therefore, the influence of outdoor climate on the energy savings of the dual source heat pump needs more data analysis, which would decide the feasibility of the ETGHP system in a climatic region.

Table 6 Heating performances of the dual source heat pump modules

Heat pump modules	Run	Heat output using CSG air (kW)	Power consumption of heating using CSG air (kW)	COP of heating using CSG air (-)	Run	Heat output using outdoor air (kW)	Power consumption of heating using outdoor air (kW)	COP of heating using outdoor air (-)	Run time of defrosting (h)	Power consumption of defrosting (kW)	Cooling capacity of defrosting (kW)	Total COP (-)
	time of heating using CSG air (h)				time of heating using outdoor air (h)							
Module 01 of unit 1#E	10.010	96.25	21.21	4.5	6.290	69.30	21.46	3.2	0.000	0.00	0.00	4.0
Module 01 of unit 4#W	5.100	90.44	20.85	4.3	10.570	65.61	21.58	3.0	0.015	18.82	64.75	3.4
Module 01 of unit 5#E	8.860	96.46	20.12	4.8	6.900	71.73	20.73	3.5	0.000	0.00	0.00	4.2

Note: Data are selected from 9:00 Jan. 17 to 9:00 Jan. 19, 2021. The time values are accumulated values, and the others are in average.

Table 7 Heating performances of the air source heat pump modules

Heat pump modules	Run time of heating (h)	Heat output (kW)	Power consumption of heating (kW)	COP of heating (-)	Run time of defrosting (h)	Power consumption of defrosting (kW)	Cooling capacity of defrosting (kW)	Total COP (-)	During running module 01 using CSG air		
									Capacity of heating (kW)	Power consumption of heating (kW)	COP of heating (-)
Module 02 of unit 1#E	16.833	73.41	20.49	3.6	0.000	0.00	0.00	3.6	73.41	19.82	3.7
Module 02 of unit 4#W	16.720	67.39	20.67	3.3	0.061	22.42	69.16	3.2	67.39	19.64	3.4

Note: Data are selected from 9:00 Jan. 17 to 9:00 Jan. 19, 2021. The time values are accumulated values, and the others are in average.

### **4.3. Perspective and future study**

The developed ETGHP system creates enormous potential for energy savings in multi-span greenhouse heating. It makes the utmost of the differences in lighting and thermal characteristics of various greenhouses. Thus, the system has a promising application prospect in regions with multiple greenhouse structure types, such as in China, multi-span greenhouses account for 2.9% of the total greenhouse area, CSGs account for 30.5%, and plastic tunnels account for 66.6% [33]. In recent years, the planning and construction of large-scale protected horticulture farms have required multiple greenhouses to meet different cultivation functions and plant rotations. This requirement provides further opportunities for the application of energy transfer between greenhouses.

A pilot test was carried out to analyze the system running conditions and application effects, as well as the performance of heat pumps. For next stage, evaluating these effects and properties using the whole heating season as the time scale would be necessary. It may also study COPs at a system level, the efficiency of CSG excess energy use, the contribution of CSG surplus air heat collection to the heating requirements, operating characteristics of each component (e.g., fitting performance curves of the heat pump under higher grade heat sources), and economic and ecological effects. Furthermore, control rules could be discussed, supporting further study of optimal climate control of greenhouses equipped with the ETGHP system.

A systematic sizing method is established, orienting to the engineering design of the ETGHP system, most of which can apply to other heating systems. The developed models have been improved, at least at a theoretical level, and showed good performances. Generally following these models and calculations for sizing, the ETGHP system was implemented and applied successfully. However, relevant statistical analysis of local meteorological data is needed to put these models into practice, and systematic model calibration and validation are also recommended for further study.

## **5. Conclusions**

This study proposes a heating approach that utilizes energy transfer between greenhouses. The ETGHP system was designed and built to practice this approach. The system collects surplus air heat inside CSGs to heat the multi-span greenhouse, enabling greenhouse energy transfer in time and space. A pilot study showed that the running states and heating effects of the system were stable.

The dual source heat pump is the core component of the ETGHP system. Its two sets of evaporators are placed in both the CSG and ambient air, respectively, enabling the heat pump to have two heat sources and cope with different weather conditions. Accordingly, it has three operating conditions: CSG air source heating, outdoor air source heating, and defrosting. The dual source heat pump had considerable potential for energy savings. Its COP reached 4.3-4.8 when using CSG surplus air heat as the heat source, 23-26% higher than when using ambient air over the same periods. Throughout the entire course of heat collection, dual source heat pumps, switching sources based on their setting, achieved a total COP of 3.4-4.2, a 6-11% increase compared to air source heat pumps.

A systematic sizing method orienting to the engineering application of the ETGHP system was put forward and used to implement the system successfully. It contained a heating load model of multi-span greenhouses, a surplus air heat model of CSGs, and the key equipment selection (including the dual source heat pump, heat storage tank, and surface air cooler). The area matching was then suggested.

The heating load model of multi-span greenhouses is simple, explanatory, and completely reliable in theory. It simplifies calculation processes, only considering combined heat transfer through the envelope and air infiltration heat loss. The model redefines the heat transfer coefficient of greenhouse cover, adding radiative heat exchange between indoor radiating bodies and the sky through the cover. The hierarchical valuing method for design temperatures of indoor and outdoor air is proposed to eliminate the risk of uncertainty in extremely cold weather, enabling the model to meet requirements for air source heat pump selection. In addition, this model is compatible with greenhouses with internal and external heat insulations, and distinguishes greenhouses cultivating fruiting and leafy vegetables.

The surplus air heat model of CSGs takes indoor air as the analysis object, studying convections and air exchanges. Its development extends descriptions of the main radiative heat transfer processes among internal surfaces of the CSG envelope, indoor floor, external surface of the transparent south roof, and the sky. Meanwhile, shading influences on solar radiation received by internal surfaces of the north roof, north wall, and indoor floor are involved.

According to simulations, the available CSG surplus air heat ranged from 100.8 to 112.6 W m<sup>-2</sup> for system design. The heating load of a multi-span greenhouse with the external thermal blanket was 98.2 W m<sup>-2</sup>. The minimum area of CSGs as heat sources was suggested to be twice the multi-span greenhouse area heated by the ETGHP system, while the critical matching ratio was 2.3-2.5 based on the relationship between greenhouse energy supply and demand.

## **Data availability**

The raw data used for analysis and generating figures and tables in this study is available at Mendeley Data, <http://dx.doi.org/10.17632/wtpt7mssrn.1>.

## **Acknowledgment**

This research was funded by National Key Research and Development Program of China (project number: 2019YFE0125100) and joint UK-China: precision for enhancing agricultural productivity project (grant reference: 107459). The authors would like to thank Agricultural Bureau of Shouguang, Shouguang Jinhong Investment Development Group Co., Ltd., and Beijing HE-energy Technology Co., Ltd for providing their support when implementing the heating system designed in this study. We also thank Bo Zhou greatly for fruitful discussions on modeling and coding. Additional thanks to Katherine Hardy and Xanthea Heynes from Nottingham Trent University for proofreading the manuscript.

## **Appendix A. Supplementary description for system implementation in the case study**

### **A1. The heated multi-span greenhouse**

The multi-span greenhouse (Fig. A1) had ridges from north to south and was 52 m in length. The span was 12 m, and the gutter width was 1.6 m. The greenhouse had 12 spans, with a total length of 163.2 m in the east-west. The equipment room was at the north end of the greenhouse. Eaves height was 6.1 m, and ridge height was 8.6 m. The indoor floor sank 1 m. The height of the foundation wall above the horizontal plane was 0.85 m. The roof angle was 23°. Sidewalls consisted of three-glass and two-cavity tempered insulating glass, and the roof was covered with 5 mm diffuse scattering single-layer glass. The gutter was composed of a 50 mm polystyrene board coated with a galvanized steel sheet. The greenhouse was also equipped with an external thermal blanket and an external shading screen. The external thermal blanket consisted of a double-layer polyethylene woven cloth filled with 8 mm polyethylene foam and 200 g m<sup>-2</sup> glue-sprayed cotton, with a total thickness of about 35 mm. This greenhouse was used for tomato cultivation.



Fig. A1 Outside view of the heated multi-span greenhouse

## A2. The heat source CSGs

CSG 1# and CSG 4-6# had identical specifications (Fig. A2). The ridge height was 7 m, the net span was 16 m, and the east-west length was 265 m. The south roof angle was  $21^\circ$ , taking the upper chord of the roof truss as the benchmark. The north roof had a width of 1.5 m and a roof angle of  $40^\circ$ , with the covering soil being 2 m thick. The north wall was a trapezoidal soil wall, 6 m in height and 2-8 m in thickness. Its internal and external surfaces were protected by spraying cement mortar. CSG 2# had a ridge height of 8 m, a net span of 22 m, and an east-west length of 265 m. The south roof angle was  $18^\circ$ , and the north roof angle was  $40^\circ$ . The north roof had a width of 1.5 m, and its covering soil thickness was 2 m. The north wall was a trapezoidal soil wall with a height of 7 m and thicknesses of 2-8 m. Again, the internal and external surfaces were protected by cement mortar spraying. CSG 3# had a ridge height of 7 m, a net span of 17.5 m, and an east-west length of 265 m. The south roof angle was  $24^\circ$ . The north roof was horizontal, 1.1 m in width, with its principal material being a 45 mm polystyrene board. The north wall was inclined inward, and the angle with the indoor floor was  $78^\circ$ . Its length was 7.2 m, and it was made predominantly from a 200 mm polystyrene board. The south roofs of all the CSGs had a 0.15 mm polyolefin film cover.



Fig. A2 Outside view of a heat source Chinese solar greenhouse

### A3. The dual source heat pump module

Table A1 Performance parameters of the selected dual source heat pump module

Items	Parameters		
	Heating condition 1 (ambient air temperature 7°C, outlet water temperature 45°C)	Heating condition 2 (ambient air temperature -12°C, outlet water temperature 41°C)	
Heat pump module	Heating capacity (kW)	85.9	53
	Input power (kW)	24.2	20.4
	COP (-)	3.55	2.6
	Power supply	380V-50Hz	
	Refrigerant	R410A	
Compressor	Compressor type	Entire seal vortex type	
	Input power (kW)	22	/
Heat exchanger	Evaporator type	Finned tube heat exchanger	
	Condenser type	Shell and tube heat exchanger	
Fan	Fan type	Axial flow fan	
	Air flow (m <sup>3</sup> h <sup>-1</sup> )	27000	
	Input power (kW)	2.2	

### A4. Control scheme

The upper control of the ETGHP system was achieved by the self-developed cloud platform for the intelligent management of greenhouse cultivation. The platform connected with a plurality of local

programmable logic controllers (PLCs) through RS485 serial communication. Through hard wiring, the PLCs were then linked to various system components and sensors.

The system control scheme was as follows. The heat pump unit was controlled cooperatively by the inlet water temperature (approximates the water temperature of the heat storage tank) and time. The inlet water temperature setpoint for stopping the heat pump was  $t_{inl,up}$  (°C), and the lower deviation was  $\Delta t_{inl}$  (°C), indicating that when the inlet temperature dropped to the lower limit of  $t_{inl,up} - \Delta t_{inl}$ , the heat pump started. The set of  $t_{inl,up}$  was different during the day and night to save energy. During the run-time of the heat pump, if the CSG air temperature was higher than the reference temperature of generating surplus air heat  $t_{gC,up}$ , the heat pump would run under the CSG air source heating condition with a lower deviation of  $\Delta t_{gC}$  (°C). Otherwise, the heat pump would run under the outdoor air source heating condition. The heat pump switched heat sources from ambient air to CSG air at the threshold temperature of  $t_{gC,up}$ , and from CSG air to ambient air at  $t_{gC,up} - \Delta t_{gC}$ . When the air temperature inside the multi-span greenhouse was low at night, the combined air conditioning unit was turned on, and upper and lower limits of the indoor air temperature were set to  $t_{g,up}$  and  $t_{g,low}$  (°C), respectively. The fan was controlled by PID frequency conversion. Its output frequency responded to the real-time greenhouse heating requirement and circulating water temperature at the heat-dissipating terminal, with upper and lower limits of  $\phi_{low}$  and  $\phi_{up}$  (Hz). To avoid the risk of irreversible crop freezing injury, which could potentially be caused by the freezing crack of circulating water pipes or water flow faults of heat pumps, the water pump for heat pump heating was typically turned on during overwintering production. The water pump for heat release applied linkage control with the fan and ran with constant pressure.

The correlation mechanism of system components was that the running fan was controlled by air temperature inside the multi-span greenhouse. Meanwhile, the fan running affected temperatures of the heat storage tank and the heat pump circulating water, thus deciding the running of the heat pump.

## References

- [1] Zhou C. Modern greenhouse engineering. 2nd ed. Beijing: Chemical Industry Press; 2010.
- [2] de Zwart F, Vanthoor B, Koreneef S. Tuinbouw zonder fossiele energie (No. WPR-853). Wageningen: Wageningen Plant Research, Business unit Glastuinbouw; 2019.
- [3] Stanghellini C, Van 't Ooster B, Heuvelink E. Greenhouse horticulture: technology for optimal crop production. The Netherlands: Wageningen Academic Publishers; 2019.
- [4] Ahamed MS, Guo H, Tanino K. Energy saving techniques for reducing the heating cost of conventional greenhouses. Biosyst Eng 2019;178:9-33. <http://doi.org/10.1016/j.biosystemseng.2018.10.017>
- [5] Gupta MJ, Chandra P. Effect of greenhouse design parameters on conservation of energy for greenhouse environmental control. Energy 2002;27:777-94. [http://doi.org/10.1016/S0360-5442\(02\)00030-0](http://doi.org/10.1016/S0360-5442(02)00030-0)
- [6] Vadiée A, Martin V. Energy management strategies for commercial greenhouses. Appl Energy 2014;114:880-8. <http://doi.org/10.1016/j.apenergy.2013.08.089>

- [7] Sigrimis N, Anastasiou A, Rerras N. Energy saving in greenhouses using temperature integration: a simulation survey. *Comput Electron Agric* 2000;26:321-41. [http://doi.org/10.1016/S0168-1699\(00\)00083-1](http://doi.org/10.1016/S0168-1699(00)00083-1)
- [8] Van Beveren PJM, Bontsema J, Van Straten G, Van Henten EJ. Minimal heating and cooling in a modern rose greenhouse. *Appl Energy* 2015;137:97-109. <http://doi.org/10.1016/j.apenergy.2014.09.083>
- [9] van Beveren PJM, Bontsema J, van Straten G, van Henten EJ. Optimal control of greenhouse climate using minimal energy and grower defined bounds. *Appl Energy* 2015;159:509-19. <http://doi.org/10.1016/j.apenergy.2015.09.012>
- [10] van Beveren PJM, Bontsema J, van Straten G, van Henten EJ. Optimal utilization of a boiler, combined heat and power installation, and heat buffers in horticultural greenhouses. *Comput Electron Agric* 2019;162:1035-48. <http://doi.org/10.1016/j.compag.2019.05.040>
- [11] Cuce E, Harjunowibowo D, Cuce PM. Renewable and sustainable energy saving strategies for greenhouse systems: A comprehensive review. *Renew Sustain Energy Rev* 2016;64:34-59. <http://doi.org/10.1016/j.rser.2016.05.077>
- [12] Tong Y, Kozai T, Nishioka N, Ohyama K. Greenhouse heating using heat pumps with a high coefficient of performance (COP). *Biosyst Eng* 2010;106:405-11. <http://doi.org/10.1016/j.biosystemseng.2010.05.003>
- [13] Aye L, Fuller RJ, Canal A. Evaluation of a heat pump system for greenhouse heating. *Int J Therm Sci* 2010;49:202-8. <http://doi.org/10.1016/j.ijthermalsci.2009.07.002>
- [14] Hassanien RHE, Li M, Tang Y. The evacuated tube solar collector assisted heat pump for heating greenhouses. *Energy Build* 2018;169:305-18. <http://doi.org/10.1016/j.enbuild.2018.03.072>
- [15] Benli H, Durmuş A. Evaluation of ground-source heat pump combined latent heat storage system performance in greenhouse heating. *Energy Build* 2009;41:220-8. <http://doi.org/10.1016/j.enbuild.2008.09.004>
- [16] Luo J, Xue W, Shao H. Thermo-economic comparison of coal-fired boiler-based and groundwater-heat-pump based heating and cooling solution – A case study on a greenhouse in Hubei, China. *Energy Build* 2020;223:110214. <http://doi.org/10.1016/j.enbuild.2020.110214>
- [17] Chai L, Ma C, Ni J-Q. Performance evaluation of ground source heat pump system for greenhouse heating in northern China. *Biosyst Eng* 2012;111:107-17. <http://doi.org/10.1016/j.biosystemseng.2011.11.002>
- [18] Ozgener O, Hepbasli A. Experimental performance analysis of a solar assisted ground-source heat pump greenhouse heating system. *Energy Build* 2005;37:101-10. <http://doi.org/10.1016/j.enbuild.2004.06.003>
- [19] Awani S, Kooli S, Chargui R, Guizani A. Numerical and experimental study of a closed loop for ground heat exchanger coupled with heat pump system and a solar collector for heating a glass greenhouse in north of Tunisia. *Int J Refrig* 2017;76:328-41. <http://doi.org/10.1016/j.ijrefrig.2017.01.030>
- [20] Zhang J. Geothermal energy, waste heat energy and heat pump technology. Beijing: Chemical Industry Press; 2014.
- [21] Hassanien RHE, Li M, Lin WD. Advanced applications of solar energy in agricultural greenhouses. *Renew Sustain Energy Rev* 2016;54:989-1001. <http://doi.org/10.1016/j.rser.2015.10.095>
- [22] Gorjian S, Calise F, Kant K, Ahamed MS, Copertaro B, Najafi G, et al. A review on opportunities for implementation of solar energy technologies in agricultural greenhouses. *J Clean Prod* 2021;285:124807. <http://doi.org/10.1016/j.jclepro.2020.124807>
- [23] Song M, Deng S, Dang C, Mao N, Wang Z. Review on improvement for air source heat pump units during frosting and defrosting. *Appl Energy* 2018;211:1150-70. <http://doi.org/10.1016/j.apenergy.2017.12.022>
- [24] Wu C, Liu F, Li X, Wang Z, Xu Z, Zhao W, et al. Low-temperature air source heat pump system for heating in severely cold area: Long-term applicability evaluation. *Build Environ* 2022;208:108594. <http://doi.org/10.1016/j.buildenv.2021.108594>
- [25] Esen H, Inalli M, Esen M, Pihtili K. Energy and exergy analysis of a ground-coupled heat pump system with two horizontal ground heat exchangers. *Build Environ* 2007;42:3606-15. <http://doi.org/10.1016/j.buildenv.2006.10.014>
- [26] Vadiée A, Martin V. Energy analysis and thermoeconomic assessment of the closed greenhouse – The largest commercial solar building. *Appl Energy* 2013;102:1256-66. <http://doi.org/10.1016/j.apenergy.2012.06.051>
- [27] Bouadila S, Kooli S, Skouri S, Lazaar M, Farhat A. Improvement of the greenhouse climate using a solar air heater with latent storage energy. *Energy* 2014;64:663-72. <http://doi.org/10.1016/j.energy.2013.10.066>
- [28] Gourdo L, Fatnassi H, Tiskatine R, Wifaya A, Demrati H, Aharoune A, et al. Solar energy storing rock-bed to heat an agricultural greenhouse. *Energy* 2019;169:206-12. <http://doi.org/10.1016/j.energy.2018.12.036>
- [29] Yang S-H, Rhee JY. Utilization and performance evaluation of a surplus air heat pump system for greenhouse cooling and heating. *Appl Energy* 2013;105:244-51. <http://doi.org/10.1016/j.apenergy.2012.12.038>
- [30] Righini I, Vanthoor B, Verheul MJ, Naseer M, Maessen H, Persson T, et al. A greenhouse climate-yield model focussing on additional light, heat harvesting and its validation. *Biosyst Eng* 2020;194:1-15. <http://doi.org/10.1016/j.biosystemseng.2020.03.009>
- [31] Katzin D, Marcelis LFM, van Mourik S. Energy savings in greenhouses by transition from high-pressure sodium to LED lighting. *Appl Energy* 2021;281. <http://doi.org/10.1016/j.apenergy.2020.116019>
- [32] Vadiée A, Martin V. Energy management in horticultural applications through the closed greenhouse concept, state of the art. *Renew Sustain Energy Rev* 2012;16:5087-100. <http://doi.org/10.1016/j.rser.2012.04.022>
- [33] Institute of Protected Agriculture AoAPaE. Greenhouse Data, <http://data.sheshiyuanyi.com>; 2020 [accessed 1 December 2020].
- [34] Liu X, Wu X, Xia T, Fan Z, Shi W, Li Y, et al. New insights of designing thermal insulation and heat storage of Chinese solar greenhouse in high latitudes and cold regions. *Energy* 2022;242:122953.

<http://doi.org/10.1016/j.energy.2021.122953>

[35] Lu W, Zhang Y, Fang H, Ke X, Yang Q. Modelling and experimental verification of the thermal performance of an active solar heat storage-release system in a Chinese solar greenhouse. *Biosyst Eng* 2017;160:12-24.

<http://doi.org/10.1016/j.biosystemseng.2017.05.006>

[36] Xia T, Li Y, Wu X, Fan Z, Shi W, Liu X, et al. Performance of a new active solar heat storage–release system for Chinese assembled solar greenhouses used in high latitudes and cold regions. *Energy Rep* 2022;8:784-97.

<http://doi.org/10.1016/j.egy.2021.12.005>

[37] Xu W, Guo H, Ma C. An active solar water wall for passive solar greenhouse heating. *Appl Energy* 2022;308:118270.

<http://doi.org/10.1016/j.apenergy.2021.118270>

[38] Xu W, Song W, Ma C. Performance of a water-circulating solar heat collection and release system for greenhouse heating using an indoor collector constructed of hollow polycarbonate sheets. *J Clean Prod* 2020;253:119918.

<http://doi.org/10.1016/j.jclepro.2019.119918>

[39] Zhao S, Zhuang Y, Zheng K, Ma C, Cheng J, Ma C, et al. Thermal performance experiment on air convection heat storage wall with cavity in Chinese solar greenhouse. *Trans Chin Soc Agric Eng* 2018;34:223-31.

<http://doi.org/10.11975/j.issn.1002-6819.2018.04.027>

[40] Bao E, Shen T, Zhang Y, Cao K, Cao Y, Chen D, et al. Thermal performance analysis of assembled active heat storage wall in Chinese solar greenhouse. *Trans Chin Soc Agric Eng* 2018;34:178-86. <http://doi.org/10.11975/j.issn.1002-6819.2018.10.022>

[41] Ma C, Jiang Y, Cheng J, Zhao S, Xia N, Wang P, et al. Analysis and experiment of performance on water circulation system of steel pipe network formed by roof truss for heat collection and release in Chinese solar greenhouse. *Trans Chin Soc Agric Eng* 2016;32:209-16. <http://doi.org/10.11975/j.issn.1002-6819.2016.21.028>

[42] Ling H, Chen C, Wei S, Guan Y, Ma C, Xie G, et al. Effect of phase change materials on indoor thermal environment under different weather conditions and over a long time. *Appl Energy* 2015;140:329-37.

<http://doi.org/10.1016/j.apenergy.2014.11.078>

[43] Guan Y, Chen C, Ling H, Han Y, Yan Q. Analysis of heat transfer properties of three-layer wall with phase-change heat storage in solar greenhouse. *Trans Chin Soc Agric Eng* 2013;29:166-73. <http://doi.org/10.3969/j.issn.1002-6819.2013.21.021>

[44] Guan Y, Wang T, Wei M, Liu T, Hu W, Duan S. Thermal performance experiment of heat storage wall with flat micro heat pipe array in solar greenhouse. *Trans Chin Soc Agric Eng* 2021;37:205-12. <http://doi.org/10.11975/j.issn.1002-6819.2021.03.025>

[45] Sun W, Yang Q, Fang H, Zhang Y, Guan D, Lu W. Application of heating system with active heat storage-release and heat pump in solar greenhouse. *Trans Chin Soc Agric Eng* 2013;29:168-77. <http://doi.org/10.3969/j.issn.1002-6819.2013.19.021>

[46] Sun W, Guo W, Xu F, Wang L, Xue X, Li Y, et al. Application effect of surplus air heat pump heating system in Chinese solar greenhouse. *Trans Chin Soc Agric Eng* 2015;31:235-43. <http://doi.org/10.11975/j.issn.1002-6819.2015.17.031>

[47] Tong G, Christopher DM, Li B. Numerical modelling of temperature variations in a Chinese solar greenhouse. *Comput Electron Agric* 2009;68:129-39. <http://doi.org/10.1016/j.compag.2009.05.004>

[48] Zhou C, Ding X. Outside temperature for heating load in greenhouse design. *Trans Chin Soc Agric Eng* 2008;24:161-5. <http://doi.org/10.3321/j.issn:1002-6819.2008.10.032>

[49] Razavi SH, Ahmadi R, Zahedi A. Modeling, simulation and dynamic control of solar assisted ground source heat pump to provide heating load and DHW. *Appl Therm Eng* 2018;129:127-44.

<http://doi.org/10.1016/j.applthermaleng.2017.10.003>

[50] Nagano K, Katsura T, Takeda S. Development of a design and performance prediction tool for the ground source heat pump system. *Appl Therm Eng* 2006;26:1578-92. <http://doi.org/10.1016/j.applthermaleng.2005.12.003>

[51] Deng W, Yu J. Simulation analysis on dynamic performance of a combined solar/air dual source heat pump water heater. *Energy Convers Manag* 2016;120:378-87. <http://doi.org/10.1016/j.enconman.2016.04.102>

[52] Cai J, Zhang F, Ji J. Comparative analysis of solar-air dual source heat pump system with different heat source configurations. *Renew Energy* 2020;150:191-203. <http://doi.org/10.1016/j.renene.2019.12.128>

[53] Nam Y, Ooka R, Shiba Y. Development of dual-source hybrid heat pump system using groundwater and air. *Energy Build* 2010;42:909-16. <http://doi.org/10.1016/j.enbuild.2009.12.013>

[54] Grossi I, Dongellini M, Piazzini A, Morini GL. Dynamic modelling and energy performance analysis of an innovative dual-source heat pump system. *Appl Therm Eng* 2018;142:745-59. <http://doi.org/10.1016/j.applthermaleng.2018.07.022>

[55] Lazzarin RM. Dual source heat pump systems: operation and performance. *Energy Build* 2012;52:77-85. <http://doi.org/10.1016/j.enbuild.2012.05.026>

[56] Fu J, Zhou C, Wang L. Methods for calculation of heating load in gutter-connected glasshouse. *Trans Chin Soc Agric Eng* 2020;36:235-42. <http://doi.org/10.11975/j.issn.1002-6819.2020.21.028>

[57] Tataraki KG, Kavvadias KC, Maroulis ZB. Combined cooling heating and power systems in greenhouses. Grassroots and retrofit design. *Energy* 2019;189:116283. <http://doi.org/10.1016/j.energy.2019.116283>

[58] Mariani L, Cola G, Bulgari R, Ferrante A, Martinetti L. Space and time variability of heating requirements for greenhouse tomato production in the Euro-Mediterranean area. *Sci Total Environ* 2016;562:834-44.

<http://doi.org/10.1016/j.scitotenv.2016.04.057>

- [59] Ahamed MS, Guo H, Tanino K. A quasi-steady state model for predicting the heating requirements of conventional greenhouses in cold regions. *Inf Process Agric* 2018;5:33-46. <http://doi.org/10.1016/j.inpa.2017.12.003>
- [60] ANSI/ASAE EP406.4. Heating, Ventilation and Cooling Greenhouses. USA: American Society of Agricultural and Biological Engineers; JAN2003 (R2008).
- [61] Ministry of Industry and Information Technology of the People's Republic of China. Design regulation on greenhouse heating system. Beijing: China Machine Press; 2014.
- [62] Zhang Y, Ma C, Liu Y, Han J. Numerical simulation and experimental verification of heat transfer through multi-layer covering of greenhouse. *Trans Chin Soc Agric Eng* 2010;26:237-42. <http://doi.org/10.3969/j.issn.1002-6819.2010.04.040>
- [63] Vanthoor BHE. A model-based greenhouse design method. Ph.D. thesis. Wageningen, The Netherlands: Wageningen University; 2011.
- [64] Geoola F, Kashti Y, Levi A, Brickman R. A study of the overall heat transfer coefficient of greenhouse cladding materials with thermal screens using the hot box method. *Polym Test* 2009;28:470-4. <http://doi.org/10.1016/j.polymertesting.2009.02.006>
- [65] Roy JC, Boulard T, Kittas C, Wang S. Convective and ventilation transfers in greenhouses, part 1: the greenhouse considered as a perfectly stirred tank. *Biosyst Eng* 2002;83:1-20. <http://doi.org/10.1006/bioe.2002.0107>
- [66] Stangheilini C. Transpiration of greenhouse crops: an aid to climate management. Ph.D. thesis. Wageningen, The Netherlands: Institute of Agricultural Engineering (IMAG); 1987.
- [67] Nijskens J, Deltour J, Coutisse S, Nisen A. Heat transfer through covering materials of greenhouses. *Agric For Meteorol* 1984;33:193-214. [http://doi.org/10.1016/0168-1923\(84\)90070-4](http://doi.org/10.1016/0168-1923(84)90070-4)
- [68] Yang S, Tao W. Heat transfer. 4th ed. Beijing: Higher Education Press; 2006.
- [69] Sun W, Zhou B, Xu F, Shang C, Lu C, Guo W. Performance of positive pressure fan-pad cooling system and cooling load model for Chinese solar greenhouse. *Trans Chin Soc Agric Eng* 2019;35:214-24. <http://doi.org/10.11975/j.issn.1002-6819.2019.16.024>
- [70] Zhao S, Ma C, Liu C, Zhang Y, Zhang J, Sun G. Computing method for thermal transmittance and saving ratio of heat loss in multi-layer covering of greenhouse. *Trans Chin Soc Agric Eng* 2011;27:264-9. <http://doi.org/10.3969/j.issn.1002-6819.2011.07.046>
- [71] Zhou N, Yu Y, Yi J, Liu R. A study on thermal calculation method for a plastic greenhouse with solar energy storage and heating. *Sol Energy* 2017;142:39-48. <http://doi.org/10.1016/j.solener.2016.12.016>
- [72] Hao X, Zheng J, Little C. Dynamic temperature integration with temperature drop to improve early fruit yield and energy efficiency in greenhouse cucumber production. *Acta Hort* 2015:127-32. <http://doi.org/10.17660/ActaHortic.2015.1107.17>
- [73] Li T. Theory and practice on vegetable cultivation in solar greenhouse. Beijing: China Agriculture Press; 2013.
- [74] Ahamed MS, Guo H, Tanino K. Sensitivity analysis of CSGHEAT model for estimation of heating consumption in a Chinese-style solar greenhouse. *Comput Electron Agric* 2018;154:99-111. <http://doi.org/10.1016/j.compag.2018.08.040>
- [75] Fang H, Yang Q, Zhang Y, Cheng R, Zhang F, Lu W. Simulation on ventilation flux of solar greenhouse based on the coupling between stack and wind effects. *Chin J Agrometeorol* 2016;37:531-7. <http://doi.org/10.3969/j.issn.1000-6362.2016.05.005>
- [76] Goudriaan I, Van Laar HH. Modelling Potential Crop Growth Processes. The Netherlands: Kluwer Academic Publishers; 1994.
- [77] Ma C, Zhang J, Qin M, Liu R. Theoretical analysis using the method of energy equilibrium in covering layer and validation of the overall heat transfer coefficient of greenhouse covering materials. *Trans Chin Soc Agric Eng* 2006;22:1-5. <http://doi.org/10.3321/j.issn:1002-6819.2006.04.001>
- [78] Ahamed MS, Guo H, Tanino K. Development of a thermal model for simulation of supplemental heating requirements in Chinese-style solar greenhouses. *Comput Electron Agric* 2018;150:235-44. <http://doi.org/10.1016/j.compag.2018.04.025>
- [79] Benli H. A performance comparison between a horizontal source and a vertical source heat pump systems for a greenhouse heating in the mild climate Elaziğ, Turkey. *Appl Therm Eng* 2013;50:197-206. <http://doi.org/10.1016/j.applthermaleng.2012.06.005>